UNIVERSITÀ DEGLI STUDI DI MILANO

Facoltà di Scienze Matematiche, Fisiche e Naturali
Corso di Laurea Magistrale in Matematica

MATHEMATICAL AND COMPUTATIONAL MODELS FOR THE STUDY OF AUTOREGULATION PHENOMENA IN THE HUMAN RETINAL MICROVASCULAR NETWORK

Relatore: Dr.ssa Paola CAUSIN
Correlatore: Prof. Riccardo SACCO

Tesi di Laurea di:
Laura ORIGGI
Matricola n. 773414

Anno Accademico 2010/2011

Contents

Introduction

The circulatory system is responsible for supplying every tissue in the body with sufficient oxygen and nutrients. Tissue demands vary according to factors such as metabolism, growth or injuries. Small arteries and arterioles regulate the amount of blood flow supplied to tissue by changing their diameters: this capability is called *autoregulation*. One of the parts of the human body whose arterioles can autoregulate is the retina. Defective or irregular autoregulation in the retina has been proved to be connected with wide-spread pathologies like diabetes and glaucoma, which makes its study relevant.

The aim of this work is to investigate mathematical models for this phenomenon, an to couple it with existing network model for the retinal microvasculature.

In the first chapter we give a brief anatomical description of the retina, with an in depth look at its circulatory system and microvasculature. The retinal vasculature is divided in three layers, the deeper the layer, the smaller the vessels. A general introduction to the phenomenon of autoregulation and the mechanisms which activate it is also presented.

The second chapter presents an existing mathematical modelization of the retinal microvasculature, characterized by a dichotomous symmetric branching system, a fractal dimension and a branch exponent which defines the relation between the length and radius of a branch segment. The microvasculature is divided into a given number of hierarchical generations, and the resulting equations system gives all the hemodynamic parameters of the network for each level (pressure, blood flow, resistance and blood viscosity). In particular, we point out the model analogies with electrical circuits, which allows to implement a compact MATLAB code to compute the hemodynamic parameters for each generation.

The third chapter approaches the problem of autoregulation from a theo-

retical and mathematical point of view: after a brief overview of the attempts to mathematically model autoregulation, a recent model by Arciero et al. is analyzed more deeply. This autoregulation model is based on a system of ordinary differential equation, and involves as state variables the diameter of the vessels which autoregulate, and their muscular activation tone. The main factors of autoregulation - myogenic, shear-stress, and metabolic - are considered, and their influence on the system is analyzed by varying the involved parameters. A MATLAB code is implemented to analyze the behavior of arteriolar diameters in time by solving the ODE system.

The fourth chapter is an attempt at coupling the network system introduced in chapter 2 with the autoregulation system introduced in chapter 3. To do so, a single MATLAB code is implemented, in which at each pressure step given as input at the first hierarchical generation of the model, the network is solved and all its relative parameter found, but before passing at the successive pressure level the newfound parameters are used to communicate with the autoregulatory system until, after a given number of iterations, convergence is reached. The code is used to perform several tests, which investigate the effects on the network reaction to different levels of pressure, but also to the presence of more or less numerous vessels which can autoregulate, the presence of autoregulation anomalies, the total resistance of the network.

In the fifth and final chapter, the autoregulation models are coupled with homogenized Darcy models. Two possible approaches are discussed: microscale and macroscale model applied in different retinal layers and hierarchical mixture theory in all the layers. After a first introductory part where Darcy' law and capillary models are introduced, the concept of macroscale and microscale models for tissue perfusion are presented. Particular attention is paid to the microscale model, which is used to model blood perfusion in retinal capillary beds. Alternatively, the microvascular system is supposed to have a hierarchical structure, but this time every hierarchical level is modeled according to Darcy's law. This generates a system of PDE, where in addition to the time and space usual variables, we have a hierarchial variable which represent the perfusion from a hierarchical level to the lower one. A first draft of the coupling of this model with autoregulation is given - the effective code which simulates the coupling could be a possible goal for future investigations on this subject.

Chapter 1

Circulation in the retina and autoregulation

1.1 Anatomical overview of the retina.

The retina is a light-sensitive tissue lining the inner surface of the eye. The optics of the eye create an image of the visual world on the retina, which serves much the same function as the film in a camera. Light striking the retina initiates a cascade of chemical and electrical events that ultimately trigger nerve impulses. These are sent to various visual centers of the brain through the fibers of the optic nerve. In vertebrate embryonic development, the retina and the optic nerve originate as outgrowths of the developing brain, so the retina is considered part of the central nervous system (CNS) and is actually brain tissue - that is why often their vasculature and hemodynamic parameters are treated as if they were the same.

.

In the center of the retina there is the *optic nerve*, an oval white area measuring about 2x15mm; from the center of this optic nerve radiate the major blood vessels of the retina. Approximately 15mm to the left of the disc a blood vessel-free reddish spot can be seen, called the *fovea*, which is the center of an area know as *macula*. The circular field of 6mm around the fovea is considered the central retina, while the area beyond this is the peripheral retina. The total retina is a circular disc of dimensions between 30 and 40mm.

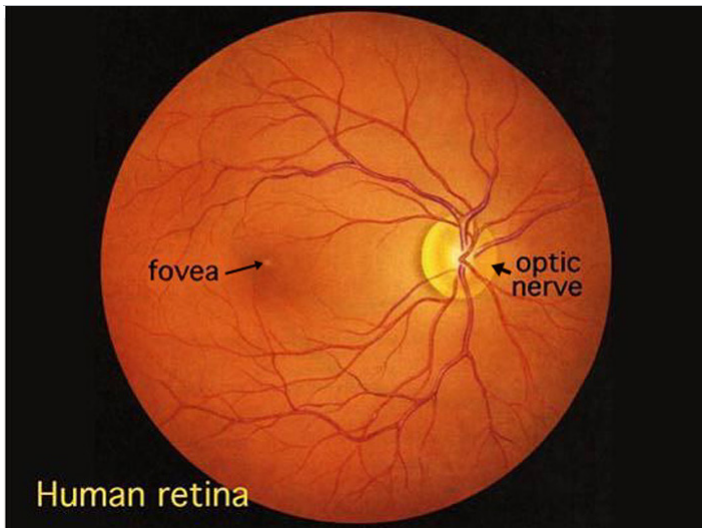

Figure 1.1: View of the human retina (seen though an opthalmoscope)

1.2 Retinal vascular network.

The only arterial blood supply to the inner retina is from the *central retinal artery* (CRA), that runs along the inferior margin of the optic nerve sheath and enters the eye at the level of the optic nerve head. (see Figure 1.2 and 1.3). Within the optic nerve, the artery divides to form the inferior/superior nasal and temporal arteries, which supply the four quadrants of the retina. The retinal venous branches are distributed in a similar fashion. The major arterial and venous branches and the successive divisions of the retinal vasculature are present in the nerve fiber layer close to the internal limiting membrane. It is important to point out that the retinal arterial circulation in the human eyes is a *terminal* system with no arteriovenous anastomoses (communication between vessels) or communication with other arterial systems: thus, the blood supply to a specific retinal quadrant comes exclusively from the specific retinal arteries and veins that supply that quadrant, and any blockage of blood supply result into infarction.

As the large arteries extends in the retina towards the periphery they divide to form arteries with progressively smaller diameters, until they reach the point where they return continuously with the venous drainage system. This process of division happens either dichotomously or at right angles to the original vessels. The terminal arteries and venules form an extensive *capillary network* in the inner retina as far as the external border of the inner nuclear layer (see Figure 1.4). The retinal vasculature is structured in

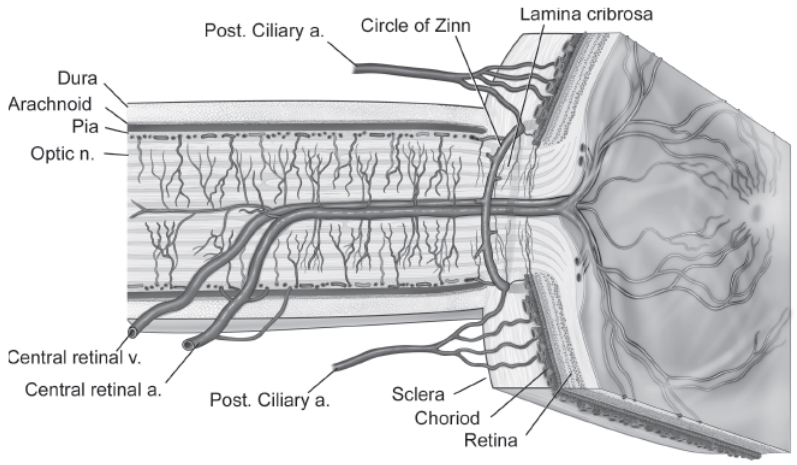

Figure 1.2: Sectional detail of the retina along the superior-inferior axis of a left human eye through the optic nerve, showing details of the vascular supply in this location.

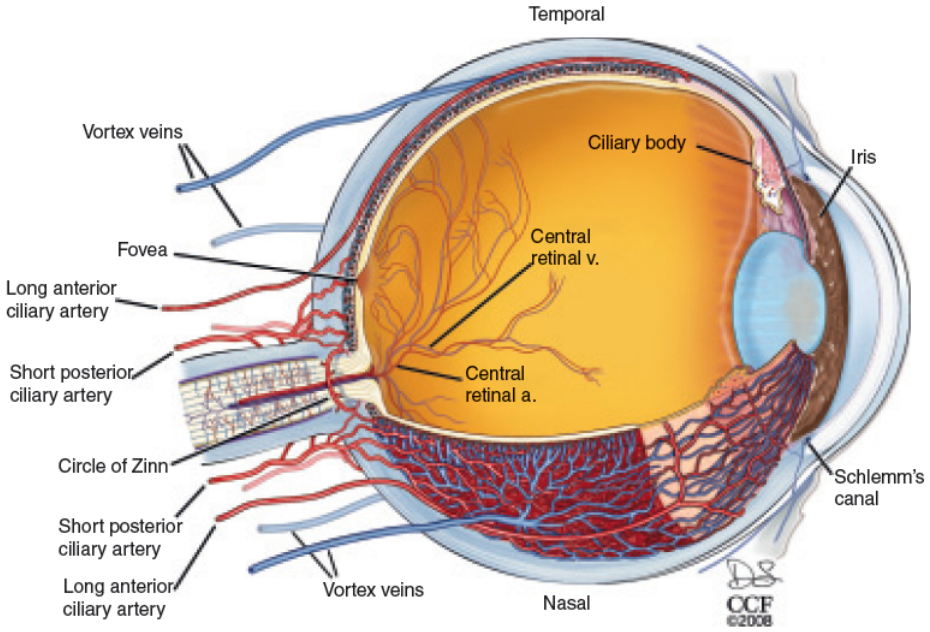

Figure 1.3: Sectional view of the human eye, showing the major blood vessels supplying the retinal choroid and anterior segment.

three distinct layers: the superficial (innermost) layer, the intermediate layer and the deep layer. The larger vessels lay in the innermost layer, whereas a plexus of capillaries occupy the other two layers with precapillary arterioles and postcapillary venules linking them to larger vessels. The superficial layer is located in the nerve fibre and ganglion cells layer and the deep one lies in the inner nuclear layer (see Figure 1.4).

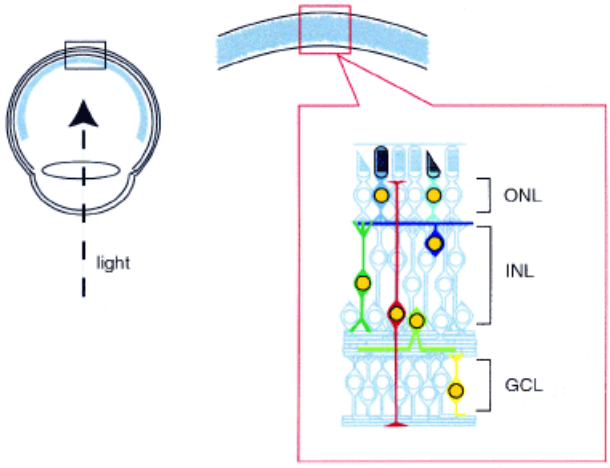

Figure 1.4: A schematic view of the retinal layers. The ONL, or outer nuclear layer, contains rod (light blue) and cone (aqua blue) photoreceptors. The INL, or inner nuclear layer, contains horizontal cells (dark blue), bipolar cells (dark green), and amacrine cells (marsh green). The GCL, or ganglion cell layer, contains ganglion cells (yellow).

The rate of blood flow through the retinal circulation is approximately 1.6-1.7ml/g, with a mean circulation time of 4.7 seconds. Blood flow of the arterioles in the superficial layer is directed to the intermediate and deep layers of the retina.

Arteries and veins physiology. In the human retina arteries and veins accompany each other, but they are distinguished based on the branching pattern and the size of the vessels. *Pattern.* The arteries tend to have 'Y-shape' branches with arms of equal diameter at the equator and at the periphery of the retina. They give rise to side-arm branches which then progressively divide into dichotomous branches of arterioles. The arterioles for a 'non-uniform delivering type' branching pattern, and give rise to capillaries. The non-uniform delivery branching is also known as random terminal branching. As in the arteries, side-arm branches also arise from the veins,

and give rise to venule branches. Unlike the arterioles, the venules are more likely to have a 'conveying type' branching pattern, which is also known as strictly asymmetric branching. There are veins which are sensitively bigger than other, and they have a 'T-shape' and give uneven size to the whole veins network. The arterioles with the delivery branching pattern are more spaced out in comparison with the vessels with the conveting branching pattern. *Measurements.* The arteries around the optic nerve are approximately 100μm in diameter, with 18μm thick walls - then they decrease in diameter, until the branched arteries lying in the deeper retina reach 15μm. The major branches of the central veins close to the optic disk have a lumen of nearly 200μm with a thin wall made up of a single layer of endothelial cells having a thin basement membrane (0.1μm). The lack of smooth muscle cells in the venular vessel wall results in a loss of a rigid structural framework for such vessels, resulting in shape-changes under condition of sluggish blood flow (e.g, diabetes) or with increased venous pressure. The retinal arteries have a thicker muscolar layer, which allows increased constriction in response to pressure and chemical stimuli.

Bridge vessels. Blood flow of the superficial layer containing large vessels is mostly directed to the vasculature at the intermediate and deep layers of the retina, as it is shown in Figure 1.5. But in addition, some of the blood in the arterioles of the superficial layer is sent to venous system directly via bridge vessels (i.e. without passing through the capillary network in the intermediate and deep layers.) Such pathway is named as direct arteriovenous connection, and can be observed along the mainstreams of the veins with nearby arterioles in the superficial layer. The diameter of these arteriovenous vessels is larger than the one of capillaries.

Capillaries physiology. *Pattern.* The retinal capillary network is spread throughout the retina, diffusely distributed between the arterial and venous systems in the intermediate layer and in the deep layer, and it is anostomotic. The capillaries are connected in tri-junction connection pattern, in which each capillary is connected to two other capillaries. The capillaries either for a 'loop' shape if they are distributed in the same layer, or move transversely to connect vessels in the other layers. In the human retina a regional variation of the density of capillary distribution is reported: the capillary distribution at the equator region is denser than that in the peripheral region. *Measurements.* There are three specific area of the retina that are devoid of capillaries, for example the 400μm wide area centered around the fovea, and the one adjacent to the major vessels. The capillaries network extends as far peripherally as retinal arteries and veins. The retinal capillary lumen is extremely small(3.5-6μm).

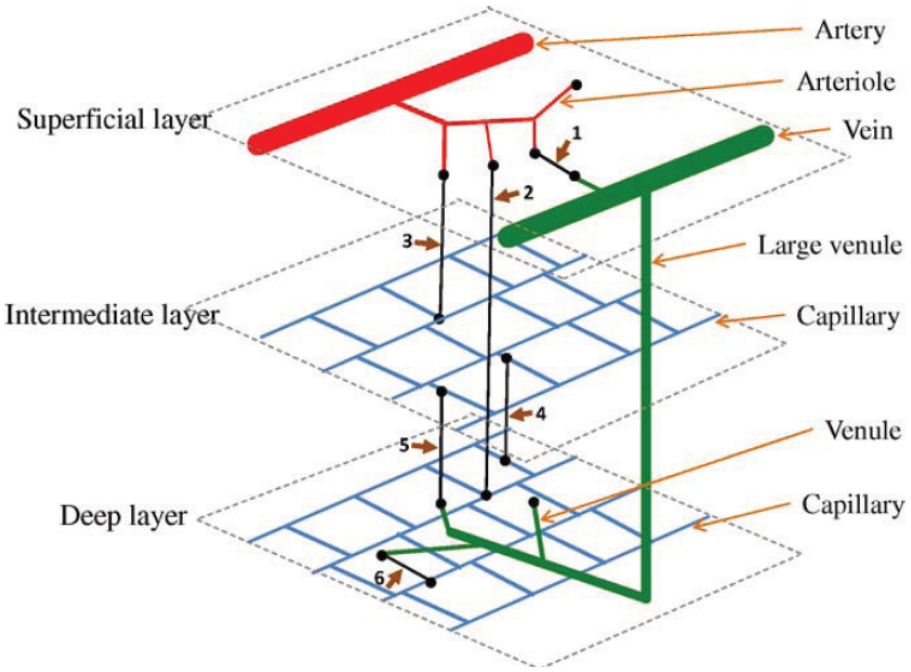

Figure 1.5: Schematic presentation of the retinal layers and the connection between vessels. (Figure taken from [22])

1.3 The phenomenon of autoregulation

The ability of vascular beds to maintain a relatively constant blood flow over a large range of arterial pressures is known as *vascular autoregulation*. The need of maintaining a constant blood flow is due to the fact that blood supplies adequate nutriment to the tissue, and that must remain guaranteed despite variations in metabolic demand, driving pressure of blood flow, oxygen or carbon dioxide content of blood. Regulation of nutrient supply to tissues involves in general both systemic controls (eg, sympathetic nervous system activation) and local factors modifying smooth muscle tone.
In retinal circulation systemic controls have only a minor influence, while local factors (eg, nitric oxide (NO), prostaglandine, endothelin) dominate regulation. This local factors will be examined for their control on total blood flow to the retina.

1.3.1 Pressure autoregulation

Intraocular pressure (IOP) is the fluid pressure inside the eye, and it is mainly determined by the coupling of the production of aqueous humor and the drainage of aqueous humor. Changes in ocular perfusion pressure (defined as the arterial pressure in the ocular vessels minus the IOP), occur routinely in daily life, as mediated by stress- and exercise induced elevations in mean arterial pressure, by nocturnal reductions in arterial pressure, and by diurnal variation in IOP. When changes in perfusion pressure occur, local vascular constriction or dilation causes vascular resistance to reciprocally increase or decrease, thereby maintaining a constant nutrient supply; this constitutes the autoregulatory response. Because increments in brachial artery (the major blood vessel of the upper arm) pressure match increments in ophthalmic artery pressure, retinal pressure autoregulation is primarily mediated by increases in retinal vascular resistance. Of course, the plateau of constant retinal blood flow as perfusion pressure varies is limited.

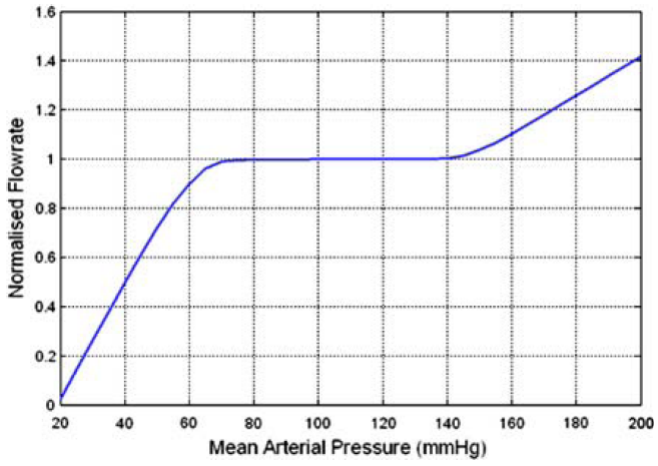

Figure 1.6: Pressure-Flowrate. The curve represent how blood flow should remain constant over a range of pressures. The value are for cerebral flowrate, similar to the retinal one. (Figure taken from [12])

Moreover, vasodilation of blood vessels in response to increased wall shear stress has been shown in many experimental studies (among the most recent [18] and [39]). Changes in blood flow alter the wall shear stress acting on the inner endothelial surface of the vessel, and shear stress is transmitted to cells mainly by the endothelial surface layer. The response of endothelial cells to increased shear stress includes increased release of NO.

1.3.2 Metabolic autoregulation and response to oxygen

Another type of autoregulation mechanism is the metabolic one, defined as the ability to elevate perfusion in response to altered tissue needs. It exists in many tissues, also in healthy retina. Vascular responses to metabolic conditions are clearly necessary for metabolic regulation of blood flow and the development of functional hyperemia (i.e. the increase of blood flow to different tissues in the body). Studies on animals ([4], [5]) have proved that for example flicker stimulation, which increases retinal metabolic demands, determine an increase of the retinal blood flow and vasodilation. Also oxygen is a crucial metabolite, and autoregulation is strongly connected with its consumption: old studies from fundus photography have proved that breathing oxygen caused a vasoconstriction of the larger retinal vessels first, and recently it has been confirmed that retinal blood flow rises and falls in inverse proportion to arterial oxygen content at a fixed arterial PCO_2 (carbon dioxide partial pressure) in healthy patients. Other arteriolar in vivo reaction are reported in [13], where a constriction as surrounding oxygen levels are increased is observed.

1.3.3 Autoregulation and glaucoma

Why is the study of autoregulation so important? Indeed it has been proved that defective autoregulation may have direct connection with pathologies like diabetes and glaucoma.

Glaucoma is an eye disease that leads to damage of the optic nerve, visual field loss and can progress to blindness. Traditionally, glaucoma and its treatment have been closely linked to intraocular pressures. In normal tension glaucoma, damage to the optic nerve occurs without any increase in intraocular pressure. Normal tension glaucoma most often occurs in the elderly and can lead to loss of sight and significant disability. . Numerous studies indicate that glaucoma patients have altered retinal circulation. Extensive morphological studies describe endothelial proliferations in the retinal vessels of glaucoma patients. In study [17] Evans et al. assert that glaucoma patients demonstrate faulty autoregulation in the retina during posture change: their CRA response to posture variation shows no change. The CRA directly feeds and is the only source of blood supply for the retinal arteries. These distal vessels nourish the retinal ganglion cells and the confluence of unmyelinated nerve fibres anterior to the lamina cribrosa.

A more recent study [9] has the objective to determine whether systemic blood pressure in the body is related to the development and progression

of normal tension glaucoma in the eye. The study aims to clarify whether subjects with episodes of hypotension (low blood pressure) at night are at increased risk for sight loss and the development of normal tension glaucoma.

Chapter 2

Mathematical models for the retinal microvascular network

The circulatory system in general, and so also the human retina we are analyzing, consists of a network of many interconnected vessels, and the flow through any segment depends not only on the flow resistance of that segment but also on the resistance of other vessels connected in series and in parallel. The multiple regulatory mechanisms, mentioned in the previous chapter, act to varying extents on segments of different size and type, and depend on variables, including flow rate, pressure and metabolic status, that are themselves dependent on the distribution of flow. Several different modes exist for transfer of information about metabolic and hemodynamic conditions between tissue and vessels and among vessels.

In a system with so many interactions and interconnections, it is difficult to unravel cause and effect and to define the role of any individual mechanism in the behavior of the system as a whole. Theoretical modeling, in combination with experimental studies, has the potential to overcome this difficulty. In a theoretical model, several observed or hypothesized mechanisms can be synthesized into a unified mathematical framework. The model can then be used to predict the overall behavior of the system, taking into account the interactions between different mechanisms occurring at the level of individual cells or segments and the interactions that arise in a network of interconnected segments. In this chapter we firstly introduce the Hagen-Poiseuille model for flow through ducts, which seems a reasonable estimation for blood flow through vessels. Then we present a model for the distribution of hemodynamic parameters in the human retina inspired by the works of Takahashi et al. [44] and Ganesan et al. [21]. The geometry of the network is based on the Murray's law, a fractal dimension and a branch exponent of

the retinal vasculature.

2.1 Hagen-Poiseuille flow

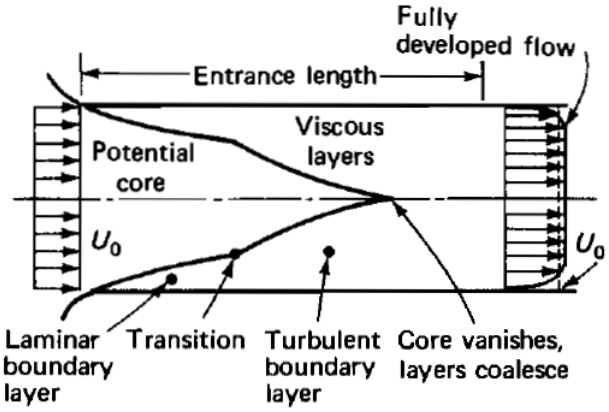

Figure 2.1: Flow in the entry region of a tube. (Figure taken from [49])

Poiseuille flows are generated by pressure gradients, with application primarily to ducts. They are named after J.L.M. Poiseuille (1840), a French physician who experimented with low-speed flow in tubes.
Consider a straight duct of arbitrary but constant shape. There will be an entrance effect, i.e. a thin initial shear layer and core acceleration (see Figure 2.1). The shear layers grow and meet, and the core disappears within a fairly short entrance length L_e. Regardless of the duct shape, the entrance length can be correlated for laminar flow in the form:

$$\frac{L_e}{D_h} \approx C_1 + C_2 Re_{D_h}$$

where $C_1 \approx 0.5$, $C_2 \approx 0.05$ and D_h is a suitable diameter scale for the duct, Re the Reinolds number.
For $x > L_e$ the velocity becomes purely axial and varies only with the lateral coordinates, so $v = w = 0$ and $u = u(y, z)$ (see Figure 2.2). The flow is then said to be *fully developed*. For fully developed flow the continuity and momentum equations for incompressible flows reduce to:

$$\frac{\partial u}{\partial x} = 0 \tag{2.1}$$

$$\begin{aligned} 0 &= -\frac{\partial p}{\partial x} + \mu\left(\frac{\partial^2 u}{\partial y^2} + \frac{\partial^2 u}{\partial z^2}\right) \\ 0 &= -\frac{\partial p}{\partial y} = -\frac{\partial p}{\partial z} \end{aligned} \tag{2.2}$$

These equations indicate that the total pressure p is a function only of x for this fully developed flow. Further, since u does not vary with x, it follows from the x-momentum equation that the gradient dp/dx must only be a negative constant. The basic equation of fully developed duct flow is thus:

$$\left(\frac{\partial^2 u}{\partial y^2} + \frac{\partial^2 u}{\partial z^2}\right) = \frac{1}{\mu}\frac{dp}{dx} = \text{const} \tag{2.3}$$

Note that the acceleration terms vanish here, since the flow is very slow.

Flow through circular pipe

The flow through a circular pipe was first studied by Hagen (1839) and Poiseuille (1840). The single variable of the model is $r^* = r/r_0$, where r_0 is the pipe radius. The Laplacian operator in polar coordinates under the hypothesis of radial symmetry and axial invariance reduces to:

$$\nabla^2 = \frac{1}{r}\frac{d}{dr}\left(r\frac{d}{dr}\right)$$

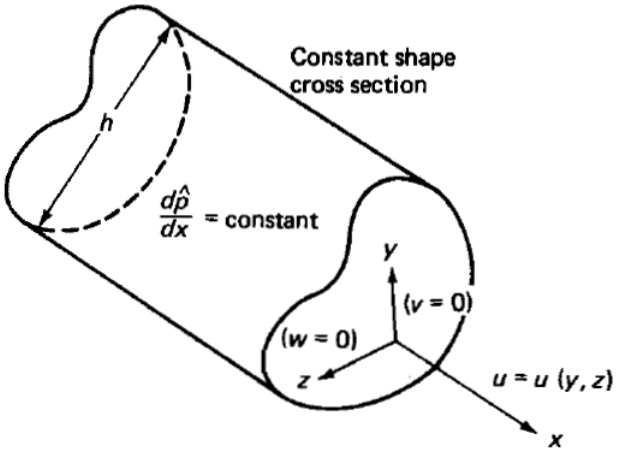

Figure 2.2: Fully developed duct flow. (Figure taken from [49])

and the solution of the fully developed equation flow $\nabla^2(u) = -1$ is

$$u = \frac{1}{4}r^2 + C_1 \ln r + C_2$$

Since the velocity cannot be infinite at the centerline we reject the logarithm term and set $C_1 = 0$. The no-slip condition is satisfied by setting $C_2 = \frac{1}{4}$. The pipe-flow solution is thus:

$$u = -\frac{dp/dx}{4\mu}(r_0^2 - r^2),$$

so that the velocity distribution in fully developed laminar pipe flow is a paraboloid of revolution about the centerline (*Poiseuille paraboloid*, see Figure 2.3). The total volume rate of flow Q is

$$Q = \int_{\text{section}} u dA$$

which for the circular pipe gives

$$Q_{pipe} = \frac{\pi r_0^4}{8\mu}\left(-\frac{dp}{dx}\right) \tag{2.4}$$

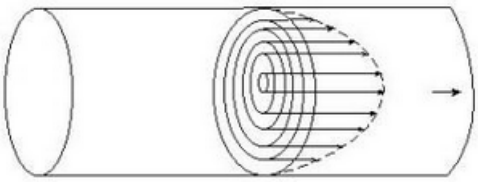

Figure 2.3: Parabolic flow in a circular pipe.

The mean velocity is defined by $v = Q/A$ and gives, in this case

$$v = \frac{r_0^2(-dp/dx)}{8\mu}$$

Finally, the *wall shear stress* is constant and given by

$$\tau_w = \mu\left(-\frac{du}{dr}\right)_w = \frac{1}{2}r_0\left(-\frac{dp}{dx}\right) = \frac{4\mu v}{r_0}, \tag{2.5}$$

Poiseuille law can be used to model the flow of blood through vessels.

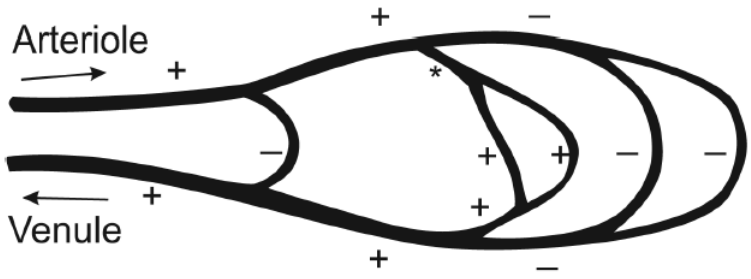

Figure 2.4: Schematic depiction of hemodynamic interaction in a microvascular network: dilatation of segment (*) causes increased flow in segment in series with the indicated segment (+) and decreased flow in parallel segments (-). (Figure taken from [41])

The importance of relationship 2.4 with regard to flow regulation is well recognized: the proportionality to r^4 implies a sensitive dependence of flow rate on diameter. For example, a reduction in lumen diameter by 10% would result in a 44% reduction in flow, if all other parameters remained constant. In reality, however, constriction of a single vessel within a network alters as well the flow, and hence the pressure drop, in other vessels in the network. The actual change in flow is less than predicted by this formula. The effects on network flow of changing the resistance of one segment are shown schematically in Figure 2.4.

2.2 Theoretical microvascular tree network

Blood flow rate in the normal microcirculation is regulated to meet the metabolic demands of the tissues, which vary widely with position and with time, but is relatively unaffected by changes of arterial pressure over a considerable range. The regulation of blood flow is achieved by the combined effects of multiple interacting mechanisms, including sensitivity to pressure, flow rate, metabolite levels and neural signals. The main effectors of flow regulation, the arterioles and small arteries, are located at a distance from the regions of tissue that they supply. Flow regulation requires sensing of metabolic and hemodynamic conditions and transfer of information about tissue metabolic status to upstream vessels.

Theoretical approaches can contribute to the understanding of flow regulation by providing quantitative descriptions of the mechanisms involved, by showing how these mechanisms interact in networks of interconnected

microvessels supplying metabolically active tissues, and by establishing relationships between regulatory processes occurring at the microvascular level and variations of metabolic activity and perfusion in whole tissues.

In their paper [44], Takahashi and Nagaoka develop a theoretical and mathematical concept to quantitatively describe hemodynamic behavior in the microvascular network of the human retina: a dichotomous symmetric branching network of the retinal vasculature is constructed, based on a combination of Murray's law and a mathematical model of fractal vascular trees. The values of hemodynamic parameters found with this model (eg. blood pressure and velocity) were consistent with in vivo measurements in the human retina and other vascular beds of small animals (see Figure 2.5). Thus this is the model we have been inspired by for our analysis.

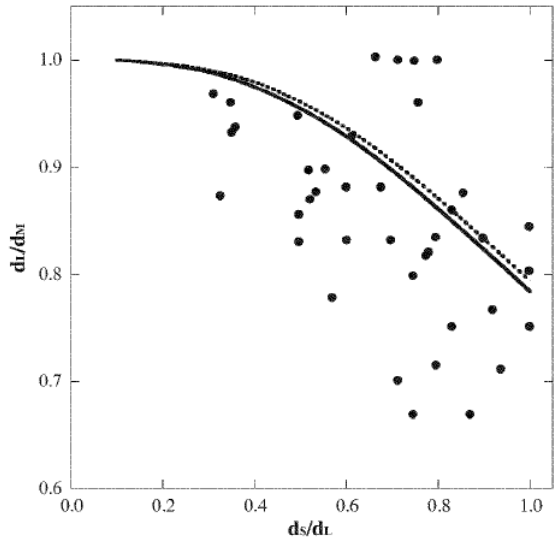

Figure 2.5: Ratio of larger daughter-branch diameters to their mother-branch diameters vs asymmetry ratio of the larger to the smaller daughter branch diameters at some bifurcations in the human retina. Dotted and solid line: curves predicted by Murray with diameter exponent 3 and 2.85 respectively. Scattered data from photographed normal human eye.(Figure taken from [44])

The optimal branching structure of a vascular tree is theoretically equivalent to $Q = kr^m$, where Q is the volumetric flow rate, r is the inner radius of the vessel segment, k is a constant, and m a junction exponent which ranges between 2.7 and 3, as shown from studies [43][42]. There is a relation between the length and the radius of a branch segment

$$L(r) = 7.4r^{\alpha} \tag{2.6}$$

where α is a branch exponent, taken in Takahashi's paper as $\alpha = 1.15$. The equation is derived from data on cerebral vessels, but it is known from studies that the vasculature of the retina and brain are similar. We choose to take $m = 2.85$, so that the equation on flow becomes $Q = kr^{2.85}$. Combining this with flow conservation, the configuration of our dichotomous vascular tree at every branching point can be expressed by

$$r_1^{2.85} = r_{2,1}^{2.85} + r_{2,2}^{2.85} \tag{2.7}$$

where r_1 is the radius of a mother branch, and $r_{2,1}$ and $r_{2,2}$ are the radii of daughter branches at the same bifurcation. The large arteriole, that originated directly from the central retinal artery (CRA), is given a generation number of 1. Branches of this generation 1 arteriole were given a generation number of 2, and subsequent generations were formed in an identical fashion until the offspring decreased about 6 μm in diameter. Individual precapillary vessel instead spread out into four true capillaries vessels, and then join again to form a single postcapillary venule.

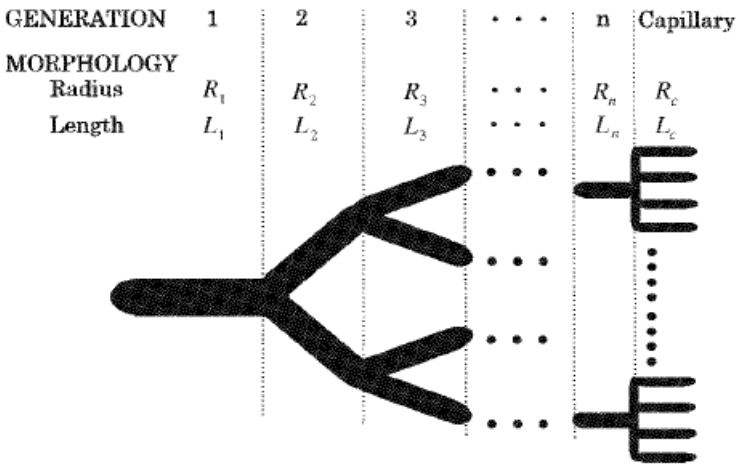

Figure 2.6: Microvascular arterial network topologically represented as a successively repeating dichotomous branching system. Each parent vessel gives rise to two offspring, each of the offspring gives rise to further two offspring, and so on. Four capillaries are assumed to divide from each precapillary. (Figure taken from [49])

In [44] Murray's law ($Q = kr^3$) was changed to $Q = kr^{2.85}$ so that it would be more suitable for application to the retinal microcirculation. The mathematical relationship between the junction exponent m and the fractal dimension of a biological tree D can be written as $m = D + \alpha$. The fractal

dimension can quantify the property of a complex vascular network, and the value of α is derived as a branch exponent from the empirical equation $L(r) = \beta r^{\alpha}$. Thus Murray's law was modified using the numerical values od D (1.70) and α (1.15) available in literature.
This modified formula can also be derived from the Hagen-Poiseuille law, when the branch length-radius relationship $L = 7.14r^{1.15}$ is substituted into Hagen-Poiseuille law $Q = \pi r^4 \Delta P/(8\mu L)$, so that the final form is $Q = \frac{k' r^4}{r^{1.15}} = k' r^{2.85}$, where k' denotes $\frac{\pi \Delta p}{7.4 \cdot 8\mu}$

2.2.1 Model equations

It is assumed that blood flow conforms to Hagen-Poiseuille's law in each vessel channel through consecutive bifurcations of the retinal microvasculature, and that the movement of material across the exchange vessels is balanced between blood and tissue.
The volumetric flow rate at the g^{th} generation blood vessel can be computed as:

$$Q_g(r_g) = \pi r_g^2 \overline{v}_g \tag{2.8}$$

where $\overline{v}$ is the mean flow velocity. The conservation of flow requires a relationship between the flow between parent vessel and daughter vessels at a bifurcation, given by:

$$Q_1(r_1) = 2Q_2(r_2) = 2^{g-1} Q_g(r_g) \tag{2.9}$$

Combining Eqs (2.8) and (2.9) gives the mean blood flow velocity in an arbitrary vessel with a cylindrical cross section:

$$\overline{v}_g = 2^{-(g-1)} \left(\frac{r_1}{r_g} \right)^2 \overline{v}_1 \tag{2.10}$$

where r_1 and $\overline{v}_1$ are the radius and mean flow velocity of the trunk vessel of generation 1. Hagen-Poiseuille's law indicates that the decrease in pressure ΔP against flow $Q(r)$ along a branch of radius r and length $L(r)$ can be written as:

$$\Delta P = \frac{8\mu(r) L(r) Q(r)}{\pi r^4} \tag{2.11}$$

where $\mu(r)$ is the apparent viscosity of blood that depends on the size of the vessel, and is supposed to follow a mathematical expression proposed by Haynes in [29],

$$\mu(r) = \frac{\mu_\infty}{(1 + \delta/r)^2} \tag{2.12}$$

where μ_∞ is the asymptotic blood viscosity, approximated at the value of $3.2 \cdot 10^2$ Poise, and $\delta = 4.29$ a constant.
Blood flow exerts a tangential force that acts on the luminal surface of the blood vessel as $\tau_w(r)$ wall shear stress

$$\tau_w(r) = \mu(r)\gamma_w(r) \tag{2.13}$$

$$\gamma_w(r) = \frac{4Q}{\pi r^3} = \frac{4\overline{v}}{r} \tag{2.14}$$

where $\gamma_w(r)$ is the shear rate at the wall surface.

2.2.2 Solution of the network

The dichotomous vascular tree built in this way has analogies with a classical electrical circuit: we can see the blood flow Q through vessels as the intensity of the current i through the conductor, the pressure drop ΔP as the potential difference measured across the conductor ΔV, and finally the conductance of the vessel as the conductance of the circuit, that is the inverse of the resistance R.

At each bifurcation node (1,2,...), for sake of symmetry the blood flow Q divides itself equally into the two daughter branches. Moreover, for the conservation of flow, as represented in Figure 2.8, for each bifurcation node the inflow must be the same as the outflow (the inflow is taken with negative sign, while the outflow with positive).

Remembering the Hagen-Poiseuille pressure drop equation:

$$\Delta P = \frac{8\mu L}{\pi r^4} Q \ ,$$

and comparing it with the equation governing the current flow through electrical network

$$\Delta V = Ri$$

we can see that the expression $\frac{8\mu L}{\pi r^4}$ is an equivalent of the resistance R for blood flow. We define its inverse:

$$G = \frac{\pi r^4}{8\mu L} \tag{2.15}$$

as *conductance* of the network. To be precise, in each bifurcation node i, where a vessel ends splitting into two daughter branches ij directed to nodes j, the node conductance is defined as follows:

$$G_{ij} = \frac{\pi r_{ij}^4}{8\mu_{ij} L_{ij}} \tag{2.16}$$

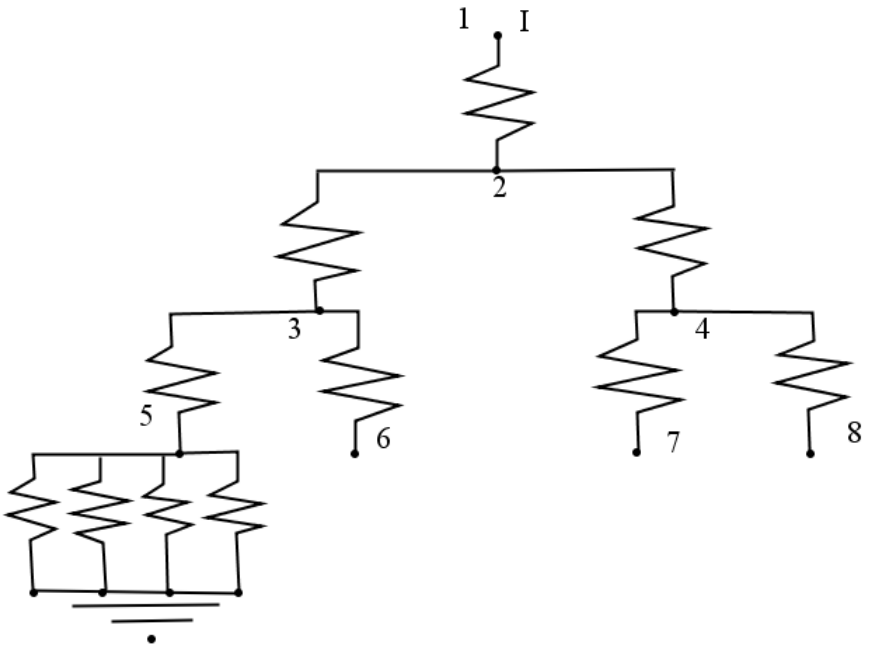

Figure 2.7: Dichotomous circuite which represents an arterial vasculature with number of generation $n_g = 3$ (i.e. number of bifurcation levels)

where r_{ij} is the radius of the vessel at generation i, L_{ij} the vessel length (the lengths of the two branches are equal for symmetry), and μ_{ij} the viscosity of the vessel.
Extending these node properties at the whole tree and combining it with the conservation of flow we get an equivalent of Kirchhoff law for blood flow:

$$\sum_{j \in Adj(i)} G_{ij}(P_i - P_j) = 0 = \sum_{j \in Adj(i)} Q_{ij} \tag{2.17}$$

where P_i and P_j are the pressures at the nodes i and j respectively. Subsequently, we can compute the blood flow in the single nodes Q_{ij} using:

$$P_i - P_j = \Delta P_{ij} = \left(\frac{\pi r_{ij}^4}{8 m u_{ij} L_{ij}} \right)^{-1} Q_{ij}$$

$$\implies Q_{ij} = \Delta P_{ij} G_{ij} \tag{2.18}$$

If we consider a simple network of vessel segments supplied by a fixed driving pressure with a single inflow and outflow segment, changing the resistance of one segment alters the flow in every segment. As in electrical

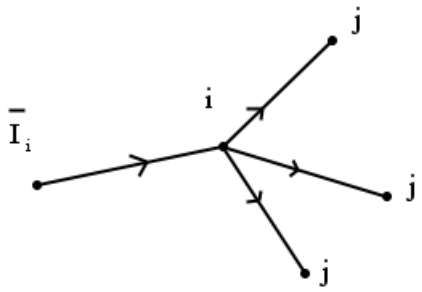

Figure 2.8: Conservation of flow (i.e. intensity of current) in a generic network tree: in each node i the outflow in the adjacent nodes must equal the inflow so that we have $\sum_{j \in Adj(i)} I_{ij} = \overline{I_i}$

circuits, in the case of segments in series, decreasing the resistance of one segment causes increased flow along the pathway containing that segment. This draws flow away from other parallel pathways, whose flow decreases. Corresponding changes in the distribution of pressure in the network occur. Vascular segments sense and respond to the levels of flow and pressure that they experience. An alteration in the distribution of flows and pressures within the network can lead to active diameter changes in other segments of the network.
Boundary nodal pressures were required to start the computation. The boundary inlet node is the artery of generation 1, where the blood flow enters the network. The boundary outlet nodes are the node where the blood flow exits the network, in our case the capillaries.

2.2.3 Numerical results

Using the model equations (2.8)-(2.14) we have computed the values of hemodynamic parameters for a network with 12 bifurcation levels, or equivalently, 13 hierarchical generation, from the feeding arteries to the terminal capillaries, confronting it with the ones for arteries and veins predicted in [44] and [21].
The diameters decreased from the large arteriole, which had a diameter of 108μm, value taken as an input data for the model, through small arterioles to precapillaries, with a diameter of 5.1μm. (Figure 2.9). Also the venular vascular network was constructed in [44] using experimental data obtained from the proximal venule, which has a diameter of 147μm - the venular diameters so obtain are a bit larger than the arteriolar ones for correspondent

generation.

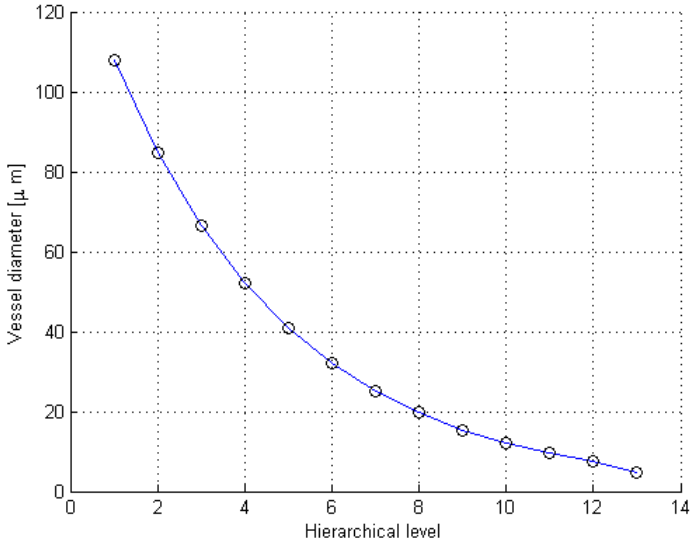

Figure 2.9: Arteriolar hierarchical level - diameter curve.

The mean flow velocity of whole blood decreased almost linearly from the first generation to the last one. Flow velocity at generation 1 was taken as an input data, and has a value of $\overline{v} = 2.055$cm/s (Figure 2.10. The mean blood flow velocity in the true capillaries dropped precipitously due to a relatively large increase in the total cross-sectional area of parallel capillaries. The mean blood flow velocity in the venular system was instead about 40% of that in the arteriolar vessels of the corresponding sizes.

The mean blood pressure at the first artery was estimated by considering the hydrostatic and frictional pressure losses from the aorta to the central retinal artery, and fixed at a value of 38.9mmHg. The intravascular pressure gradually decreased in the large arterioles (Figure 2.11), true capillaries, and venular system, whereas it steeply decreased through the terminal arterioles and precapillaries. According to [21], the pressure drop is lower for arterial segments of a larger diameter and/or of a shorter length, resulting in a higher pressure at the entry to pre-capillary vessels. The pressure in the capillaries can also vary significantly in the retinal vasculature: the regional pressure variations in capillary vasculature will initiate blood flow in angular direction.

The wall shear stress working down to vessels with a diameter of 60μm resulted almost constant, as expected from Murray's law, whereas thereafter

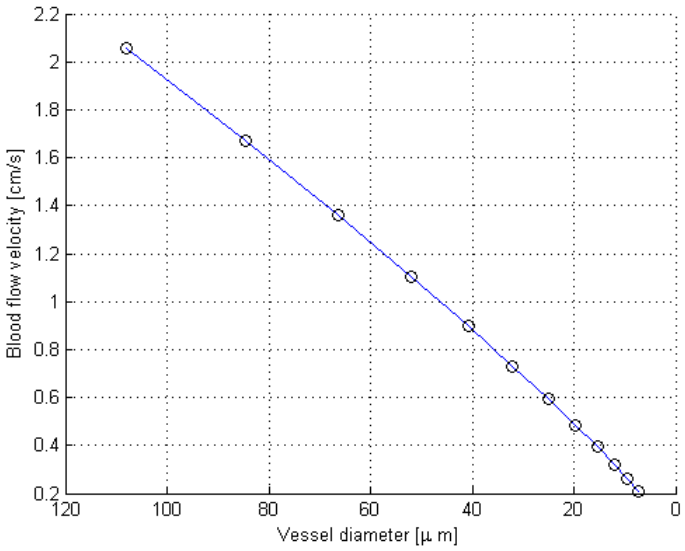

Figure 2.10: Arteriolar vessel diameter - blood flow velocity curve.

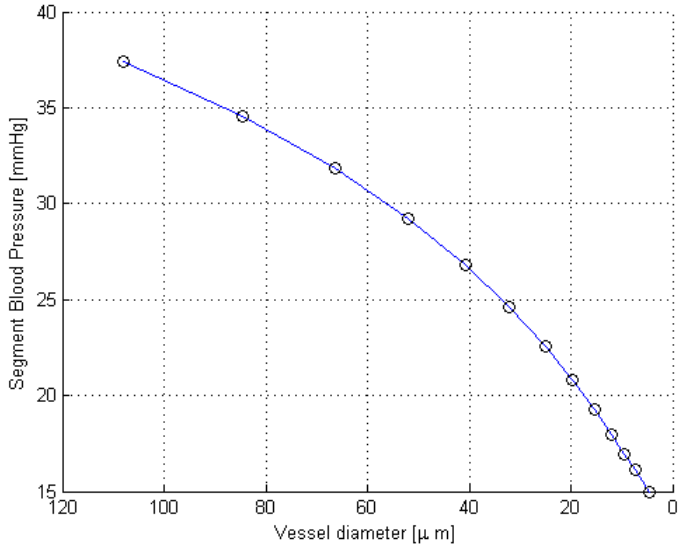

Figure 2.11: Arteriolar vessel diameter - pressure curve.

it was largely reduced until the arterial terminus due to a decrease in apparent blood viscosity because of the Fahraeus-Lindqvist effect(i.e., the viscosity of a fluid, in this case blood, changes with the diameter of the tube it travels through; in particular there's a decrease of viscosity as the tube's diameter decreases, because erythrocytes move over the center of the vessel, leaving plasma at the wall of the vessel). However, the wall shear stress at the pre-capillary vessels increased, since the apparent viscosity was increased due to the geometrical obstacle encountered by the red blood cells flowing in these narrow channels. The wall shear stress of the vessels at the pre-equator and equator region is significantly higher than that at the periphery region. This is reasonable because the fluid is flowing outwards from the center of the retina, hence the further from the center the lower the pressure is. As a result, the driving force for the flow in the arteriolar branches at the pre-equator region is higher than at the periphery, hence higher the wall shear stress.
This leads to an observation on the relationship between the high wall shear stress and the vessel wall thickness of arterial vessels near the pre-equator and equator regions. The wall of retinal arteries near the optic disc (pre-equator region) comprises five to seven layers of smooth muscles. At the equator and periphery, however, the arterial wall has only two or three and one or two muscle layers, respectively. This seems to suggest that the vessels at the pre-equator and equator regions have adapted themselves by increasing their wall thickness (i.e., smooth muscles) to sustain the higher wall shear stress.

As an important conclusion, we can add that the network model developed here can be used for predicting the development of the circulation in the retinal vasculature also under pathological condition over time, e.g. for arteriosclerosis, hypertension, diabetes, retinal vein venular occlusion. The pathological condition can be simulated by specifying changes in diameters for the required vessels to investigate the subsequent influence on the circulation within the network.

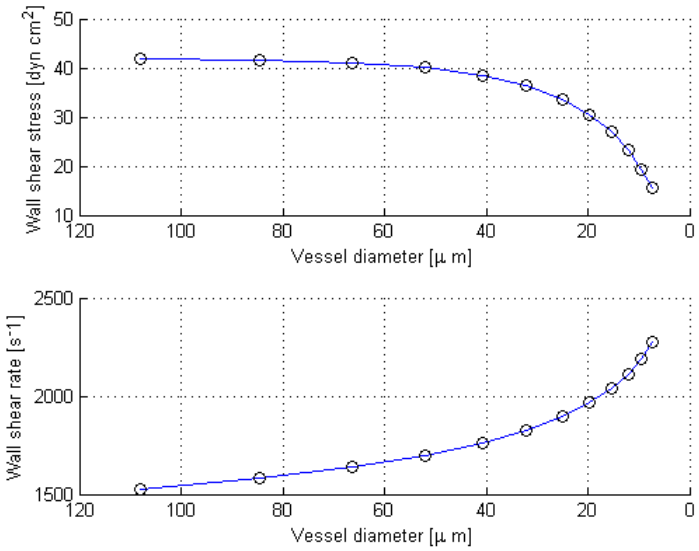

Figure 2.12: Arteriolar vessel diameter - wall shear stress and vessel diameter - shear rate curves.

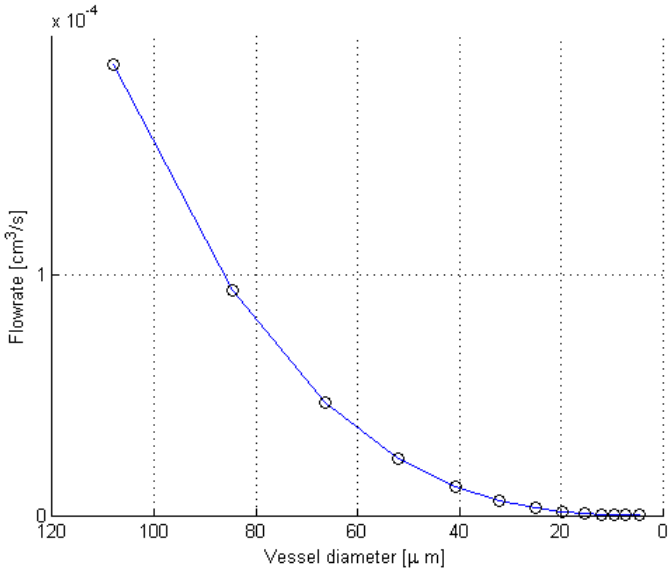

Figure 2.13: Arteriolar vessel diameter - flowrate curve.

Chapter 3

Mathematical models for blood autoregulation in the retina

In this chapter we will provide a general overview on the most important attempts at modeling the autoregulation phenomenon, to then study more deeply the one presented in [2], which is based on a system of ordinary differential equations. Finally the presented model will be implemented in MATLAB to simulate the effect of autoregulation on a single arteriolar vessel.

Arteriolar diameter is controlled by contraction or relaxation of vascular smooth muscle (VSM). The level of tone generated by a vascular smooth muscle cell (SMC) depends on several factors, including its length and tension, local level of metabolites and signaling molecules, communication with other cells via gap junction, and neural inputs. Ideally, theoretical simulations of flow regulation should be based on an integrated model for the responses of an individual VSM to all these stimuli. Such a model is not available, but some aspects of cellular responses have been considered theoretically.
A model for the electrophysiology and mechanics of SMCs was developed by Gonzales-Fernandez and Ermentrout in [23], in which the dynamics of membrane potential, potassium and calcium ion conductances and intracellular calcium binding were considered, as the active/passive length-tension relationship of smooth muscle. As typical for muscle cells, the maximum active tension that can be generated increases and then decreases with increasing length of the active element. This behavior was represented by a modified Gaussian function. The actual active tension was assumed to be equal to the maximal tension multiplied by a factor between zero and one that depends dynamically on intracellular calcium level. Myogenic effects were simulated by assuming that one of the parameters in the model, defining the voltage dependent variation in calcium conductance, is a function of intravascular

pressure. The model predicted a myogenic response, i.e., a decrease in vessel diameter with increasing pressure above 50 mmHg.
Yang et al. in [50] developed a model for SMCs incorporating both electrochemical and chemomechanical subsystems. A Hodgkin-Huxley type model was used to describe membrane electrochemistry, and a multi-state model was used for calcium-induced calcium release. The SMC model was then used in a vessel-level model of the myogenic response. Results were presented for one case predicting myogenic constriction similar to that observed in cerebral vessels. Subsequently in [51] they developed a new model for the nitric oxide/cGMP pathway in SMCs. Nitric oxide (NO) is an important vasodilator substance. Effects of NO on activation and the myosin contractile system were simulated.
The *myogenic response* has been the subject of many experimental studies, particularly with regard to its role in the autoregulation of blood flow. The biophysical mechanism by which stretching of SMCs stimulates contraction has not been established. One point of debate has been whether stress (tension) or strain (elongation) is actually sensed. In a basic sense, this question is easily answered. Overall elongation of the SMC cannot be the signal for myogenic contraction, since the signal would then go to zero once the cell contracted to its original length, and constriction to less than the initial diameter (as frequently observed) would not occur. This does not, however, rule out the possibility that some component of the cell (a 'sensor element'), connected in series with contractile elements, experiences elongation under increased tension, even when the cell as a whole is shortened. This type of response was discussed first by Johnson and Intaglietta in [26] and [27], where a model for myogenic response was developed, in which the level of the tension generated depended on the relative change in intravascular pressure. It has been debated whether VSM tone variation was to be included as a variable in the model: Kuo et al. in [34] and [35] chose not to include the variation in the level of VSM tone, while the model developed by Carlson and Secomb [8] included it, as well as many other features of the above models.
Vasodilatation of blood vessels in response to increased *wall shear stress* has been often confirmed by experimental studies. Shear stress is transmitted to endothelial cells mainly by the endothelial surface layer. The response of endothelial cells to increased shear stress includes increased release of NO. Although the intracellular signaling processes have been extensively studied, the cellular mechanism responsible for mechanotransduction of shear stress remains elusive. Liao and Kuo in [36] obtained experimental data on myogenic contraction without flow but with a controlled level of wall shear stress, and developed empirical relationships to describe the observed variation of diameter. In the model of Cornelissen et al. [10] the level of tone generated

in each segment of the arterial tree was assumed to depend on concentration of NO generated by endothelial cells, which was taken as a sigmoidal function of wall shear stress.
Vascular responses to metabolic conditions are clearly necessary for metabolic regulation of blood flow and the development of functional hyperemia (increase of blood flow to different tissues in the body). Oxygen is a crucial metabolite, and arterioles in vivo react to oxygen levels, constricting as surrounding oxygen levels are increased. Jackson [25] showed that arterioles are insensitive to changes in local oxygen level within a normal physiological range. This suggested that the sensing of oxygen levels occurs in downstream vessels or in the parenchyma and initiates responses that are conducted to the arteriole. Subsequent work has supported this hypothesis. For example Ursino et al. [46] assumed that a decrease of bloodflow rate below a set point, dependent on metabolic needs, causes dilation. Primarily responsible for carrying oxygen in blood, red blood cells (RBCs) may also act as oxygen sensors and thus play a role in communicating metabolic demand, as explained in the works by Ellsworth, [15], [16]. Finally, in more recent works, Arciero et al. [1] [2] developed a theoretical model for flow regulation which includes all this kind of responses, and we are now going to take a deeper look at it.

3.1 A theoretical mathematical model for autoregulation.

Several theoretical models for the autoregulation of flow have been developed using a multicompartmental approach, in which blood is considered to flow through a number of compartments connected in series and representing different types and size of vessels.
A flow pathway through the vascular system is represented by several compartment connected in series, each comprising a set of identical, parallel arranged segments that are assumed to experience the same hemodynamic and metabolic conditions. The number of compartments is chosen according to the level of detail desired in the model and the amount of experimental data available. An example is the one introduced in [2], in which there are seven representative segments: upstream artery (A), large arteriole (LA), small arteriole (SA), capillary (C), small venule (SV), large venule (LV), and downstream vein (V) (see Figure 3.1). In general, LA and SA are considered to be vasoactive, so that they can autoregulate, while the other hierarchies of the model are considered fixed resistances. Geometric and hemodynamic parameters are defined for each compartment, but since blood flow must be

the same in each compartment, the following relationship holds:

$$Q_{tot} = n_A Q_A = n_{LA} Q_{LA} = n_{SA} Q_{SA} = n_C Q_C = n_{SV} Q_{SV} = n_{LV} Q_{LV}$$

where Q_i is the blood flow in the vessel, Q_{tot} the total flow, and n_i the number of vessels in the compartment.

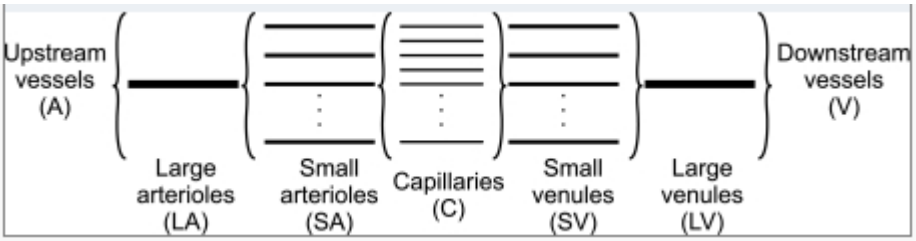

Figure 3.1: Representative segment model: the arteries and the veins branch into smaller vessels.

3.1.1 Model for myogenic response

The vascular effects of myogenic response are based on active and passive length-tension characteristics of the *vascular smooth muscle* (VSM). *The circumferential wall tension* (T) is related to pressure and diameter by the law of Laplace, assuming that vessel wall thickness is much less than vessel diameter:

$$T = \frac{PD}{2} \tag{3.1}$$

where P is the transmural pressure difference and D is the diameter (see Figure 3.2).

Tension in the vessel wall is represented as a sum of a passive component, T_{pass}, and and active component generated by the VSM. The active component can be expressed as the product of the maximal active tension that is generated at a given vessel circumference, T_{act}^{max}, and the degree of activation of the VSM tone, A. So the total tension in the vessel wall, T_{total}, is given by:

$$T_{total} = T_{pass} + AT_{act}^{max} \tag{3.2}$$

The passive tension is a non-linear function of diameter D, and is approximated by the following exponential relationship:

$$T_{pass} = C_{pass} \exp([C'_{pass}(D/D_0 - 1)]) \tag{3.3}$$

where D_0 is the passive vessel diameter at an intraluminal pressure of 100mmHg. The maximal active tension generated by the VSM cells in the vessel wall is described by a Gaussian curve

$$T_{act}^{max} = C_{act}\exp\left(-\left(\frac{D/D_0 - C'_{act}}{C''_{act}}\right)^2\right) \tag{3.4}$$

The plots for this exponential and Gaussian dependence are visualized in Figure 3.3, 3.4 and Figure 3.5.

The activation varies between 0 and 1, and is assumed to have a sigmoidal dependence on the stimulus S_{tone} determining the level of VSM tone.

$$A_{total} = \frac{1}{1+\exp(-S_{tone})} \tag{3.5}$$

The myogenic response is represented by assuming:

$$S_{tone} = C_{myo}T - C'_{tone} \tag{3.6}$$

This dependence of activation on wall tension implies that wall tension is controlled by a negative feedback mechanism: an increase in tension leads to an increase in activation. For the plot of the sigmoid A_{total} see Figure 3.6 (see table 3.1 for description of all C parameters.)

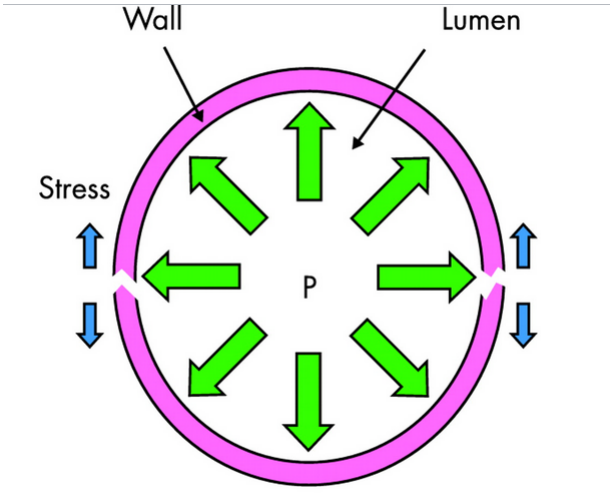

Figure 3.2: Tension in the section of a cilindrical vessel. T=PD/2, where D is the lumen diameter, P is the pressure.

3.1.2 Model for myogenic and shear-dependent responses

Changes in blood flow alter the wall shear stress τ acting on the inner endothelial surface of the vessel. According to the law of Laplace, the average circumferential shear stress in the vessel wall is given by:

$$\tau = \frac{PD}{2\eta}$$

where η is the vessel wall thickness, $\eta << D$ (see Figure 3.7). The ratio $D/2\eta$ generally ranges from 2 to 10 in LA and SA. The response of endothelial cells to increased wall shear stress includes increased release of NO, but the cellular mechanism responsible for mechanotransduction of shear stress remains elusive. In [2] the previous model for myogenic response is extended to represent responses to shear stress by including a term dependent on shear stress in S_{tone}. In particular a linear relationship between S_{tone} and the wall shear stress τ was found to fit the experimental data nearly quite well:

$$S_{tone} = C_{myo}T - C_{shear}\tau + C'_{tone} \tag{3.7}$$

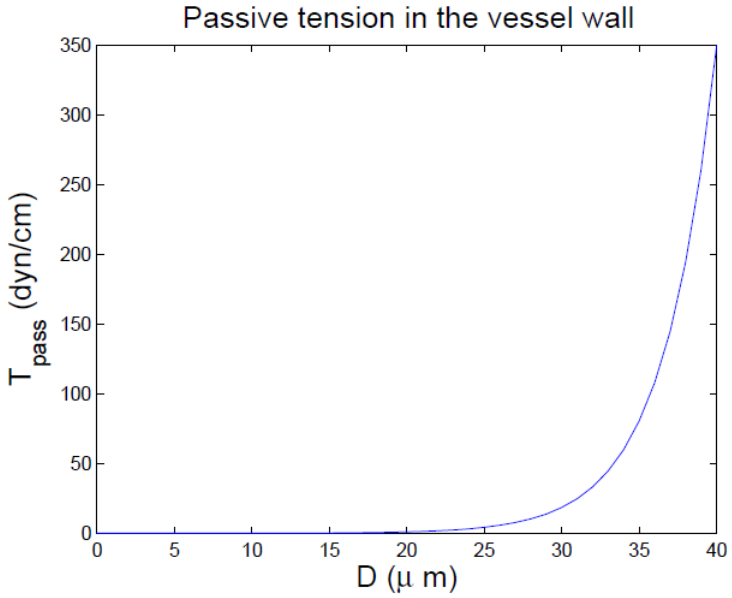

Figure 3.3: Exponential relationship between the passive tension in the vessel wall and the diameter of the vessel. For larger diameters the passive tension grows quickly, since the vessel is getting close to being maximally stretched. C'_{pass} determines the steepness of the exponential curve. (Figure taken from [19])

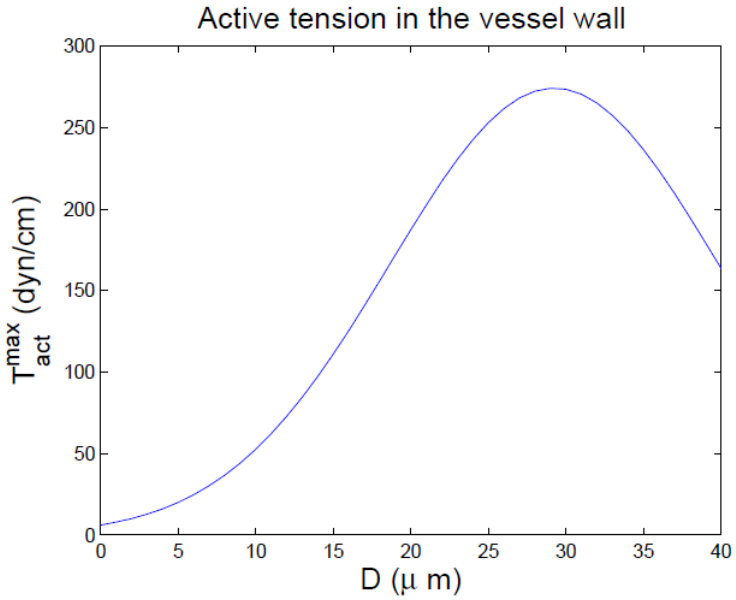

Figure 3.4: Gaussian relationship between the active tension in the vessel wall and the diameter of the vessel. C_{act} represents the peak magnitude, C'_{act} the peak location, C''_{act} the curve width. (Figure taken from [19])

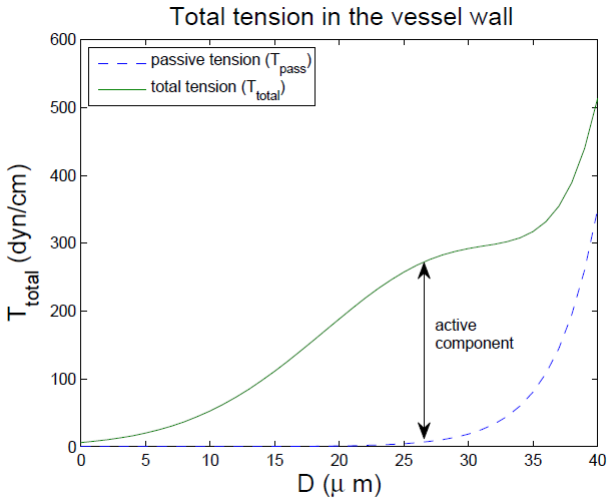

Figure 3.5: The curve shows the difference between the total tension with and without the active contribution. Activation A is fixed to 1. (Figure taken from [19])

Parameter	unit	Description
C_{myo}	cm/dyn	VSM activation tension sensitivity
C_{shear}	cm^2/dyn	VSM activation shear stress sensitivity
C_{meta}	$\mu M/cm$	VSM conducted response sensitivity
C'_{tone}		VSM constant
C''_{tone}		VSM constant
C_{pass}	dyn/cm	passive tension strength
C'_{pass}		passive tension sensitivity
C_{act}	dyn/cm	maximally active VSM peak tension
C'_{act}		maximally active VSM length dependence
C''_{act}		maximally active VSM tension range

Table 3.1: Parameter values defining arteriolar activation and diameter

Note that the summation of the new terms is carried out before the sigmoidal dependence is applied to activation, to guarantee that A still ranges from 0 to 1, under all conditions.

3.1.3 Model for myogenic, shear-dependent and metabolic responses

Red blood cells (RBCs) respond to oxygen level by releasing ATP at a rate that depends on their oxyhemoglobin saturation level. This ATP release may

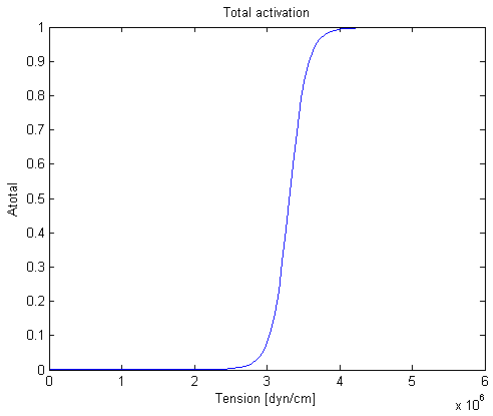

Figure 3.6: The curve shows the sigmoid dependence of A_{total} from the vessel wall tension. C_{myo} determines the steepness of the sigmoidal curve, C'_{tone} the tension at half-maximal activation $A = 0.5$.

initiate a conducted response that travels upstream and triggers arteriolar vasodilatation.
Conducted response is assumed to exponentially decay in [2] with a constant length L_0. At each point in the network, a signal is generated at the vessel wall in proportion to the local concentration of ATP in the plasma. This signal is summed from the end of the LV to the midpoints of the LA and SA in order to obtain the conducted response, $S_{CR}(x)$ that reached the large and small arterioles respectively. The summation is represented by the integral of the ATP concentration along the vascular pathway, including exponential decay of the signal in the upstream direction:

$$S_{CR}(x_{mp,k}) = \int_{x_{mp,k}}^{x_{end}} e^{\frac{-(y-x_{mp,k})}{L_0}} C(y)dy \tag{3.8}$$

where $x_{mp,k}$ is the midpoint of the compartment k=LA or SA, and X_{end} is the end point of the LV. Parameter values are given in Table

This signal is multiplied by a sensitivity factor, C_{meta}, to account for its effect on VSM activation with respect to the other contributory regulatory mechanism. The resulting expression for S_{tone} so becomes:

$$S_{tone} = C_{myo}T - C_{shear}\tau - C_{meta}S_{CR} + C''_{tone}. \tag{3.9}$$

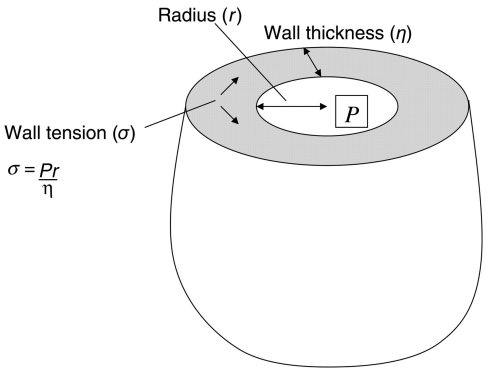

Figure 3.7: Shear Tension in the section of a vessel.

3.2 Diameter and activation level change with time

If pressure is altered, a vessel shows a rapid passive change in diameter followed by an active smooth muscle contraction or dilation to a new equilibrium diameter. This behavior can be represented by the following system of ordinary differential equations:

$$\begin{cases} \dfrac{dD}{dt} = \dfrac{1}{\tau_d}\dfrac{D_c}{T_c}(T - T_{total}) \\ \dfrac{dA}{dt} = \dfrac{1}{\tau_a}(A_{total} - A) \end{cases} \tag{3.10}$$

where T_c and D_c are the values of tension and diameter in the *control state* (i.e. the condition in skeletal muscle at a level of oxygen consumption corresponding to moderate exercise), T_{total} and A_{total} are the calculated steady state values of vessel wall tension and smooth muscle activation for given levels of pressure and oxygen demand, and τ_d and τ_a are time constants governing the rates of passive diameter and VSM activation change respectively.

3.3 Result for a single vessel: time dependent behavior of diameter.

We begin our analysis taking a single arteriole and studying its diameter change in time while applying a pulsed pressure different from the control state one. In Fry's work ([19])just the myogenic behavior is considered, in the following we instead take into account also the shear dependent and metabolic responses. We suppose the vessel is a small arteriole (SA) with diameter in control state $D_c = 14.8\mu m$. For the other C parameter used in the simulation see Table 3.2.

Pulsed pressure step. First we examine what happens to the diameter when the intraluminal pressure is increased as a pulse - that is, the pressure is held constant in the beginning until the diameter reaches its steady state for that pressure level; then it is increased to a new constant, and the new steady state of the parameter is then observed.

The results are plotted in Figure 3.10. We see that after a transient in the first $t \simeq 50s$ the diameter fix itself at a higher level than the input one. When at time $t \simeq 200s$ the pressure is increased again, after the transient we

Parameter	Value
C_{myo}, cm/dyn	0.0547
C_{shear}, cm^2/dyn	0.0258
C_{meta}, $\mu M/cm$	30
C'_{tone}	-8.031
C''_{tone}	10.66
C_{pass}, dyn/cm	316
C'_{pass}	16.702
C_{act}, dyn/cm	900
C'_{act}	0.910
C''_{act}	0.374
D_0, μm	65
D_c, μm	14.8
τ_d, s	1
τ_a, s,	60

Table 3.2: Parameter values describing oxygen transport

have a vase-contraction and the final equilibrium level is reached at $t \simeq 300s$ for ever kind of response. The equilibrium level is approximately the same one for the myogenic, shear-dependent and metabolic responses, and it is around $30\mu m$. The metabolic response has been introduced by considering the parameter of conducted response S_{CR} approximately around 0.45.

Ramped pressure step. Let's see the responses to changes in pressure which are not given by a pulse: for example, pressure can be increased linearly over time (as in Figure 3.9).

Once again before increasing the pressure we let the diameters reach their steady level for the input pressure: for every type of response we have a slight increase. After that, we have a gradual decrease of the diameter as the pressure linearly increases - when the ramp stops at $t = 350s$, the value of 110 mmHg is then held constant, and the diameter still decreases, but at a lower rate, soon fixing itself at a new steady value. In both cases the equilibrium reached by the diameter responding to metabolic effects is lower than the other twos. The activation increases reaching its limit level 1.

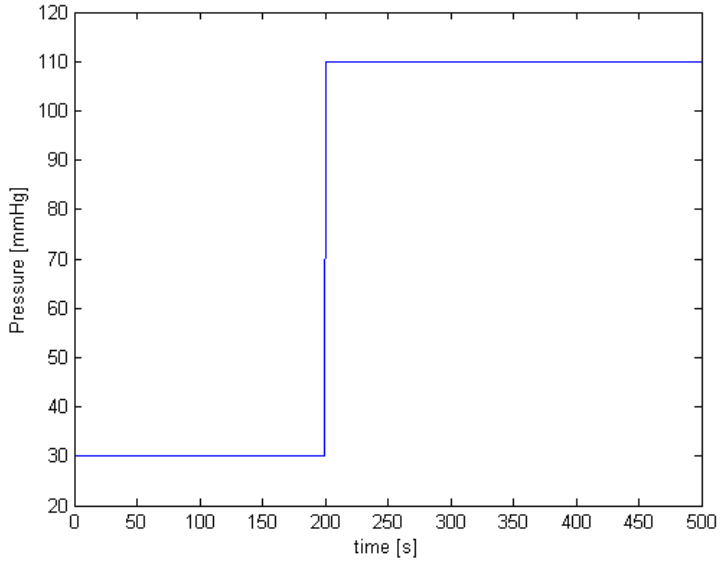

Figure 3.8: Pressure/time curve. Pressure is given as a constant pulse.

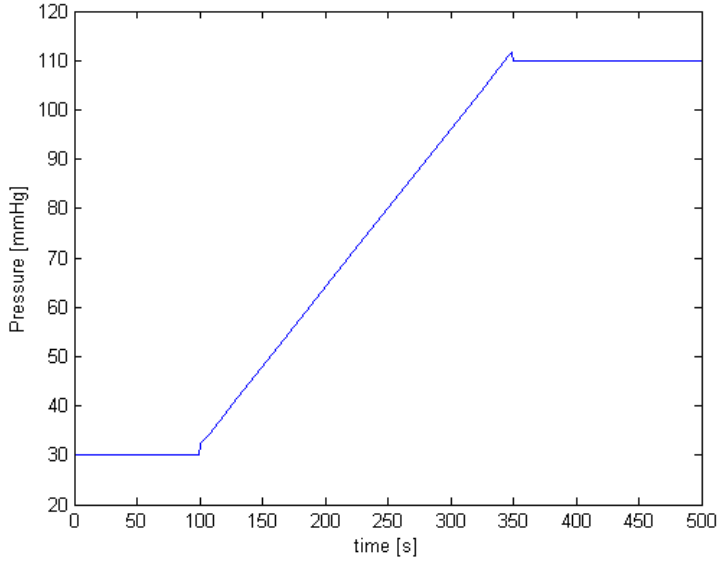

Figure 3.9: Pressure/time curve. The pulse is not constant but ramps up linearly over time.

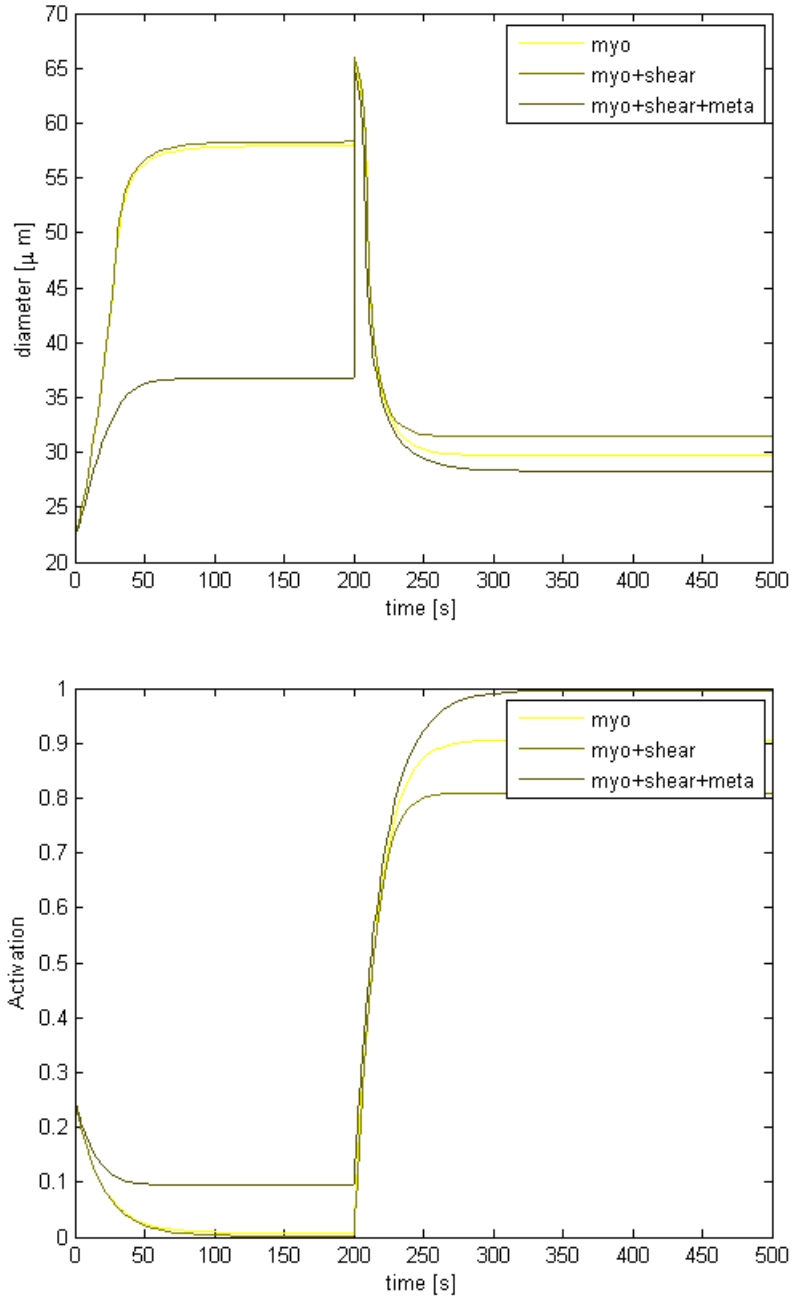

Figure 3.10: Diameter/time and Activation/time curve for model of pulsed pressure. $D_0 = 30\mu m$, $A_0 = 0.25$

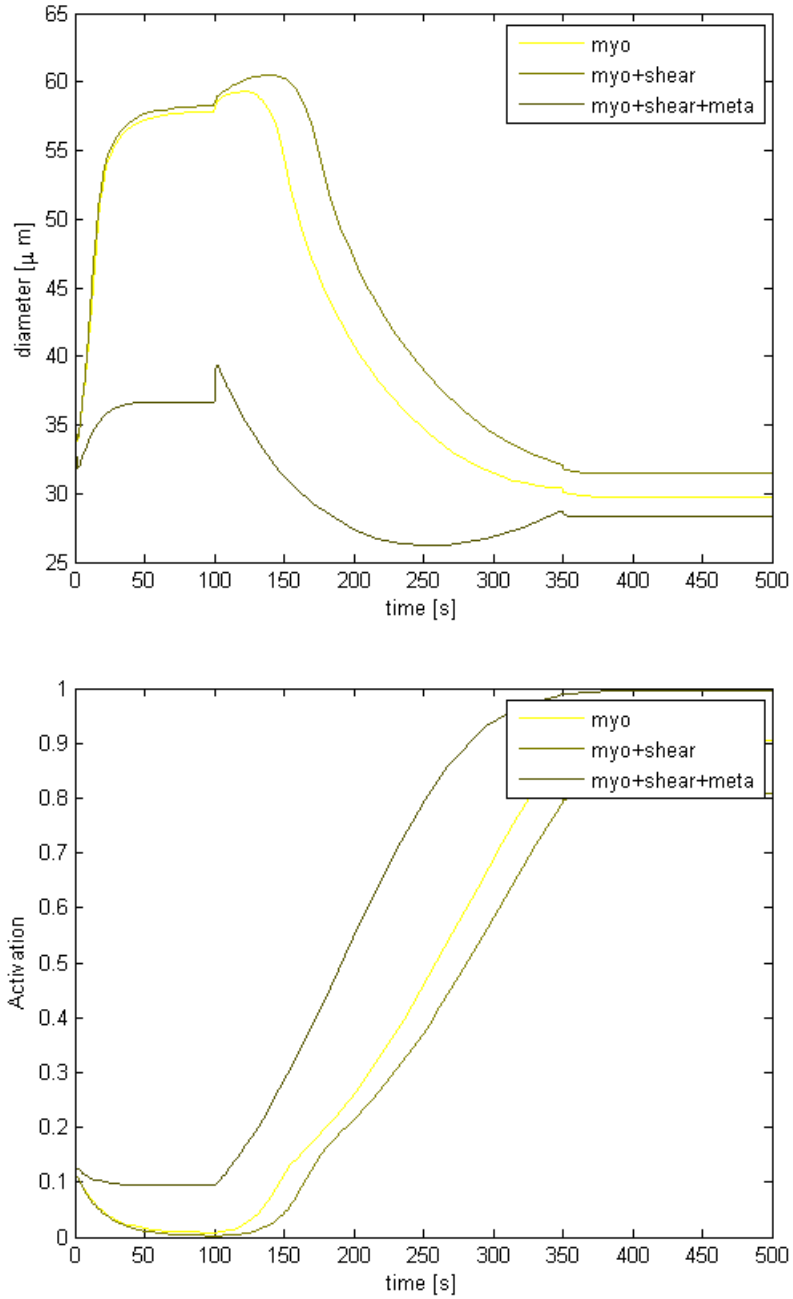

Figure 3.11: Diameter/time and Activation/time curve for model of ramped pressure. $D_0 = 30\mu m$, $A_0 = 0.10$

3.3.1 Equilibrium diameter analysis.

In this section we are going to analyze a different type of equilibrium than the one above. We are not interested anymore to see how the diameter changes in time given a constant or variable pressure, but only at taking a look at how the *equilibrium* diameter changes at different levels of pressure.

So a single arteriolar vessel is considered, along with a range of pressures: the vessel is then let go to its equilibrium diameter for each pressure value in the range, and the final values reached at each level are then summarized in a pressure vs. equilibrium diameter plot.
The pressure range chosen is [20, 180]mmHg. The equilibrium diameters found were compared with the one found using the same level of pressure but imposing $A = 0$, that is the passive case (see red line in Figure 3.12 and 3.13). The comparison between the results shows the importance of the autoregulatory mechanism. In the active case, the equilibrium value of the diameter increase for a little while (pressure $\simeq$30/40mmHg), to then begin to decrease for progressively higher values of pressure ($\simeq$ 90/110mmHg), until it finally rises again, even if not reaching again the high values it had for low pressures. In the passive case, instead, the autoregulatory mechanism is turned off, and we see that the equilibrium diameter just increases with the pressure - this is in contrast with what autoregulation suggest should happen, because there is no vaso-constriction.

The result were computed for both just myogenic response and myogenic response combined with shear-dependent and metabolic responses (Figure 3.12 and 3.13 respectively): we can see that the curves follow a similar fashion, but overall the effect on diameters in the model comprehensive of metabolic response is stronger, so that the vaso-constriction for pressure in the range of $\simeq$[40, 100] is more accentuated.

Blood flowrate has been computed in active and passive case, too, to visualize the effects of autoregulation on the effective flow in the vessel. As we have said, the goal of autoregulation is to maintain the blood flow constant in a certain range of different pressure: it is plain that in the passive case the flowrate just increase linearly with pressure, far from being constant, while with autoregulation turned on the blood flow goes through a sensible limitation.

Once again the computation has been done both for myogenic and myogenic, shear-dependent and metabolic responses combined together (Figure 3.14 and 3.15 respectively) - the limitation in the flowrate is more accentuated in the second case, and the blood flow appears so be almost constant in the pressure range from 40 to 90mmHg.

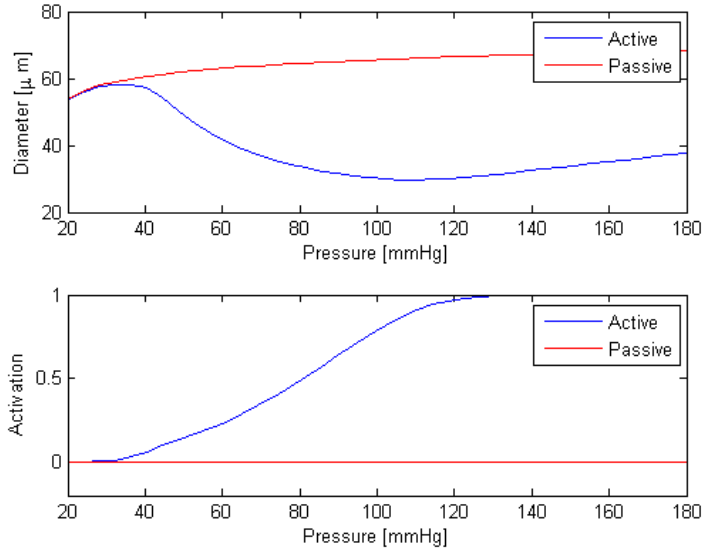

Figure 3.12: Dependance of vessel diameter on pressure in the active and passive ($A = 0$) cases. (myogenic response activated)

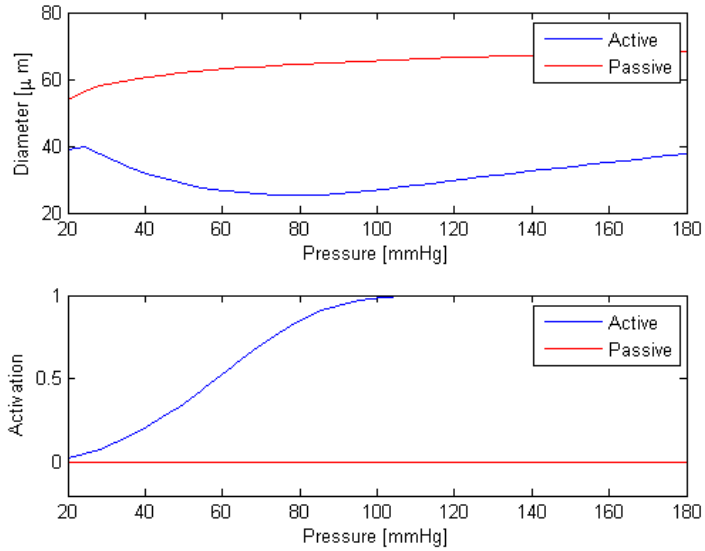

Figure 3.13: Dependance of vessel diameter on pressure in the active and passive ($A = 0$) cases. (myogenic, shear dependent and metabolic responses activated)

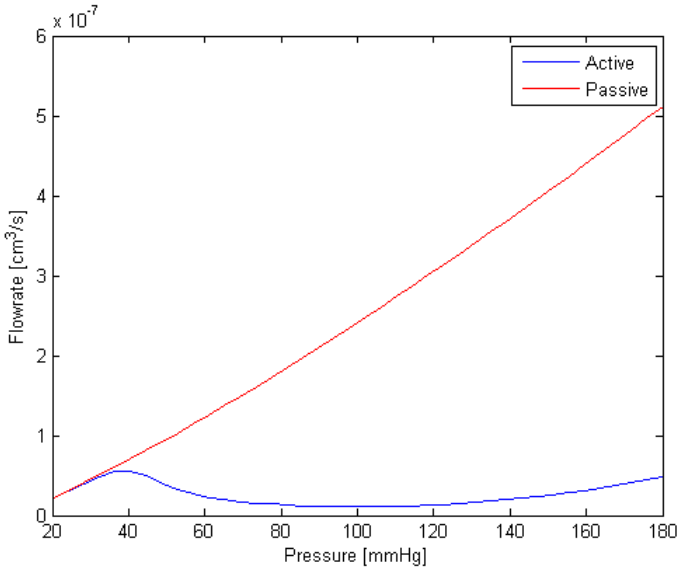

Figure 3.14: Pressure vs. flowrate curve (myogenic response).In the passive case the flowrate increased constantly in time. With autoregulation activated, instead, the vaso-contraction controls the flow.

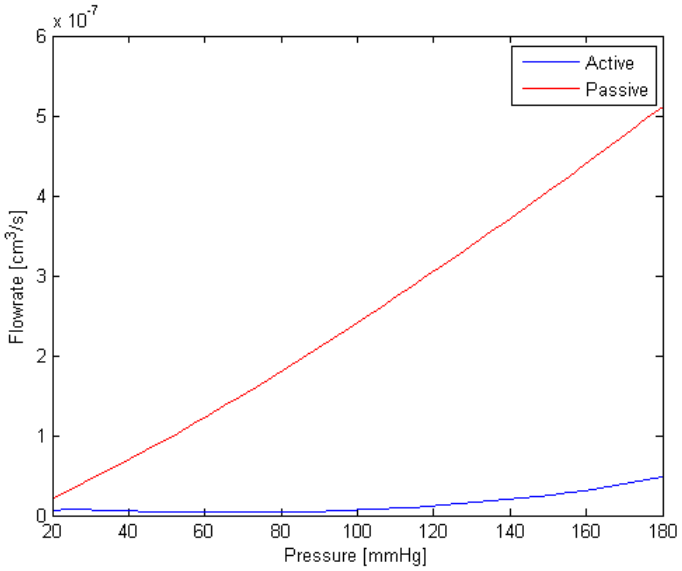

Figure 3.15: Pressure vs. flowrate curve (myogenic, shear dependent and metabolic responses).

Chapter 4

Coupling of autoregulation-network models.

Until now we have studied the effects of autoregulation on vessel diameter just in dependence of time, supposing that the systemic pressure was kept constant or ramped by external factors. We know that in the reality pressure and diameter are not independent, but they influence one another with their variations. Thus the autoregulation model should be analyzed along with the network one - or another vasculature model, as long as it computes pressure in function of diameters and other hemodynamics factors - assuming that at each step pressure and diameter should achieve a reciprocal equilibrium in the whole vascular system considered.

An example of autoregulation/network model coupling can be found in [12], where David et al. develop a non dimensional representation of both myogenic and metabolic autoregulation coupled with an asymmetric binary tree algorithm simulating the cerebro-vasculature. Despite the autoregulatory model used differs from the one considered here, the activating mechanism analyzed are the same (i.e. myogenic and metabolic), and their results show that metabolic mechanism seems to be dominant for cerebral autoregulation.

In this work we present a coupling model, which combines the autoregulation theoretical model [1] reported in Ch. 3 with the symmetrical branching tree network model [44] reported in Ch. 2. The input data of the model are: the range of inlet pressure at artery of generation 1, the number of hierarchical levels and the number of hierarchical level actually autoregulating. Different types of autoregulatory mechanism (myogenic, myogenic and shear dependent, myogenic shear-dependent and metabolic) can be selected. At each pressure level given as input at the first hierarchical generation of the model, the network is solved and all its relative parameters found, but before

passing at the successive pressure level the newfound parameters are used to communicate with the autoregulatory system until, after a given number of internal iterations, convergence is achieved. A schematic representation of the algorithm followed can be seen in Figure 4.1.

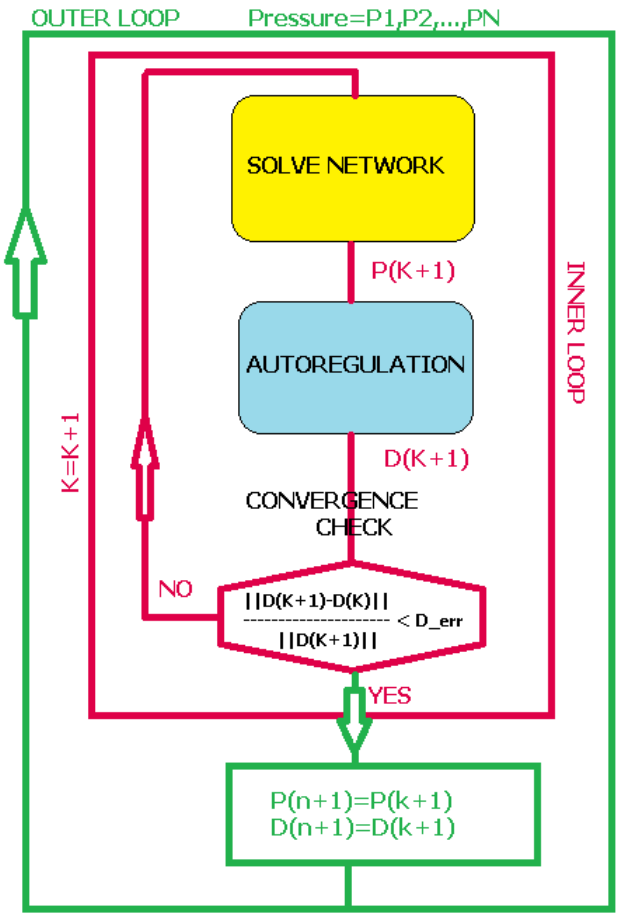

Figure 4.1: A schematic representation of the algorithm followed to implement the coupled model. The outer loop (green) iterates on pressure levels. The inner loop (pink) iterates until convergence is reached.

4.1 Numerical results

4.1.1 Effects of varying the number of hierarchies

The coupled MATLAB code has been used to investigate how the variations of the input parameters can influence the equilibrium reached by the system in each different case. As previously said, the code permits the user to choose - accordingly to computational times and memory problems - the number of hierarchical levels present in the system, i.e. the number of bifurcation level in the network tree. In Figure 4.2 the equilibrium diameters are plotted in dependence on the inlet pressure level given to generation 1 artery (we remember that for each pressure level the system is let go to equilibrium, and then the final value reached by the diameter is the one considered). First of all we notice that the trend of the diameters is similar to the one reported in Ch. 3 (see for example Figure 3.12 and 3.13), with a slight increase for lower pressure, decrease for middle pressures and a new increase for pressure above 140mmHg. These changes are more marked in larger vessels, whereas in smaller vessels the initial and final increase are barely perceptible if not totally absent. By increasing the number of hierarchical levels - in our example from 8 to 11 - the result is that the equilibrium levels of diameters increase slightly for system with a higher number of hierarchies.

4.1.2 Effects of varying the number of autoregulating levels

It is known that not every vessel in the arteriovenous system has the capability to autoregulate - for example the bigger arteries and the capillaries and precapillaries seem incapable to react to pressure changes and other mechanisms. So it is reasonable to suppose that just the hierarchical levels in the middle of our system change their diameters, and through the model we can study the changes in the equilibrium reached depending on how many levels autoregulate. In Figure 4.3 the effect of this variations are reported on two different vessels (hierarchy 3 and 5), whose diameters are plotted against pressure. The first hierarchy capable to autoregulate is supposed to be the 2nd, while the last is let to vary between the 6th and 9th. This actually influence the equilibrium level of diameter on both the vessels considered. In both levels we see that the equilibrium levels of the diameters slightly increase with the number of levels which can autoregulate: this suggest that the more vessels has the capability of autoregulate, the more the system is equilibrated, and the contraction that the single vessels have to go through

are less important.

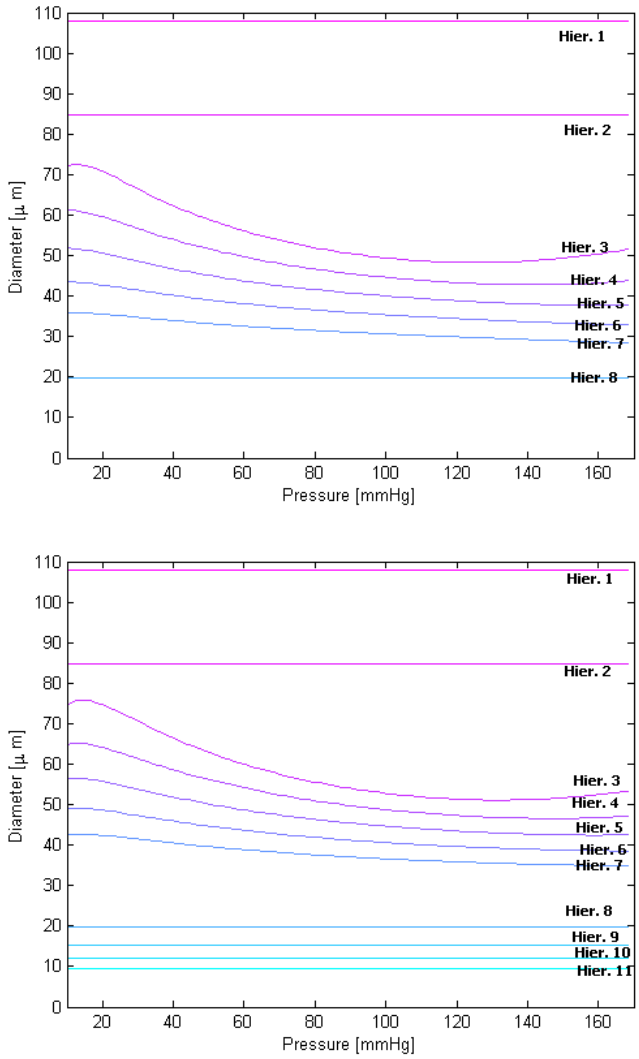

Figure 4.2: Pressure vs. diameter curves for 8 and 11 hierarchies system respectively. The hierarchies which don't autoregulate have constant diameter at every pressure level (straight lines). Only myogenic response is activated here.

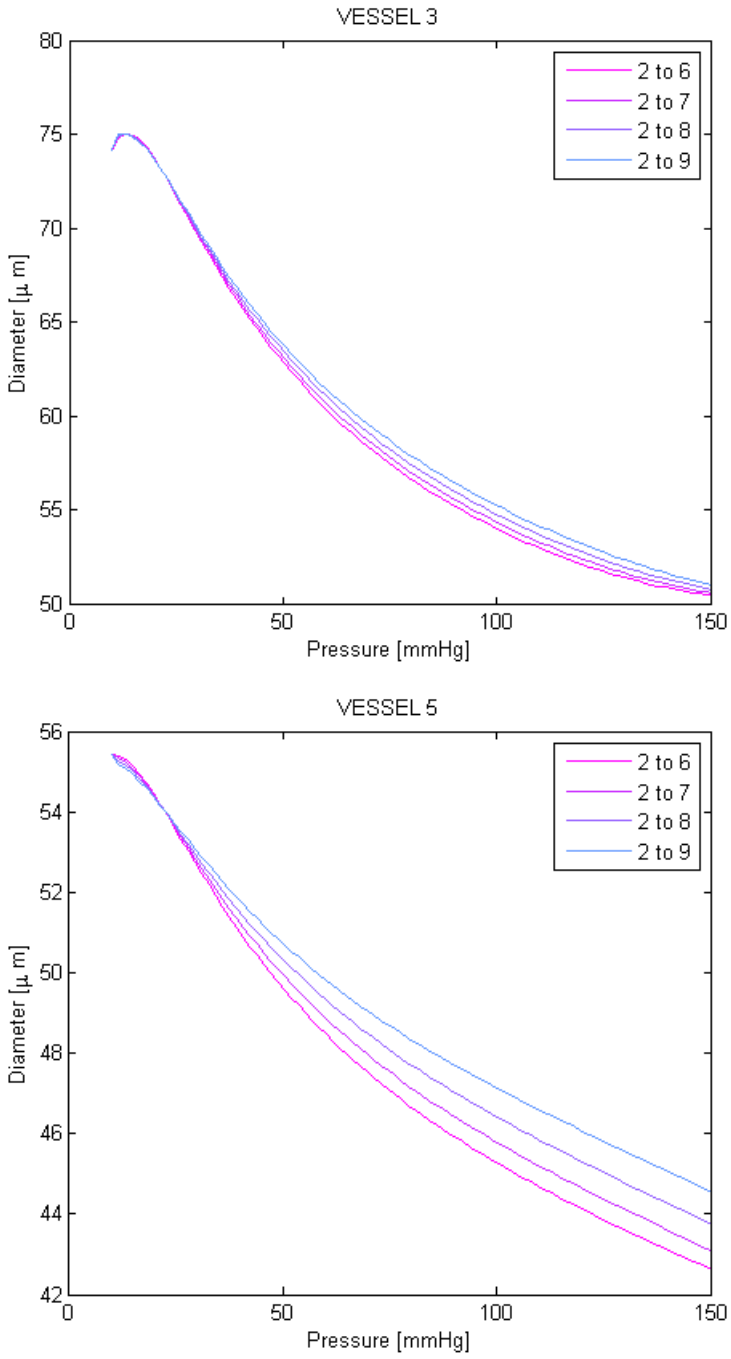

Figure 4.3: Vessel 3 and vessel 5 pressure vs. diameter plots, depending on the number of vessels which autoregulate.

4.1.3 Effects of varying the inlet pressure on mean arterial pressure in each generation.

We know that for each inlet pressure level the system is solved, and the mean pressure is found for each node of the tree, varying - usually decreasing - with the hierarchical level. The pressure at capillary level is supposed to remain always the same, independently from inlet pressure, and equal to the value of the intraocular pressure (IOP), usually around 15-20mmHg. The mean arterial pressure trends are similar for different levels of inlet pressure, but as one would have expected, the values are higher in each level when the inlet pressure is higher. In Figure 4.4 the result are plotted for a system of 8 branching levels, where the autoregulating levels are from 3 to 5.

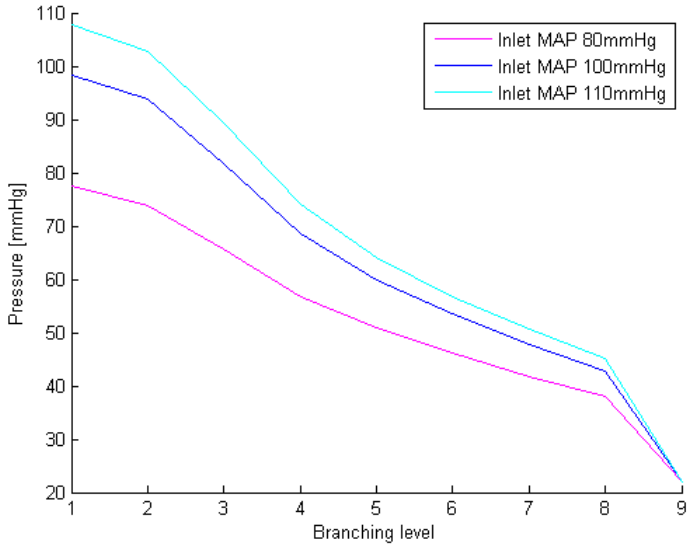

Figure 4.4: Branching level vs. pressure curves, depending on the different inlet pressure.

4.1.4 Effects of the presence of a broken/defective vessel

Until now we have supposed that all the hierarchies which could autoregulate actually did it in the proper way. But what would happen if one among these autoregulating levels was broken or defective (i.e. could not regulate at all, or could autoregulate but in a different way from the others)?

In Figure 4.5 vessel of generation 4 is supposed to be incapable to autoregulate, whereas the others (from hierarchy 3 to 7) autoregulate normally. The broken vessel is implemented in the code by deactivating the interaction with autoregulation for that specific vessel - its diameter and activation tone variations are considered equals to zero. The effect on equilibrium on vessel 6 are plotted, but we can see that the difference from the normal situation are minimal. With the presence of a broken vessel, however, the equilibrium of the other vessels diminish a bit. A possible interpretation of this kind of behavior is that the vaso-contraction is major to substitute the absent one of the broken vessel - if vessel 4 does not autoregulate the blood flow in it remains constant, and to diminish the total flow in the network the other vessels must autoregulate more strongly.
Similar result for defective vessel are reported in Figure 4.6. This time we are supposing that vessel 4 autoregulate in a sensibly slower way than the other ones, so the equilibrium diameter curve has a different trend from the other vessels. To implement this kind of behavior in the code, the autoregulation system equations for diameter and tone have been modified just for that specific level by dividing them for a factor 4. As for the effects on other vessels, we observe that the difference of equilibrium diameters between the presence or absence of defective vessels are almost imperceptible - we can conclude that the presence of a defectively autoregulating vessel is not very influencing on the system in general.

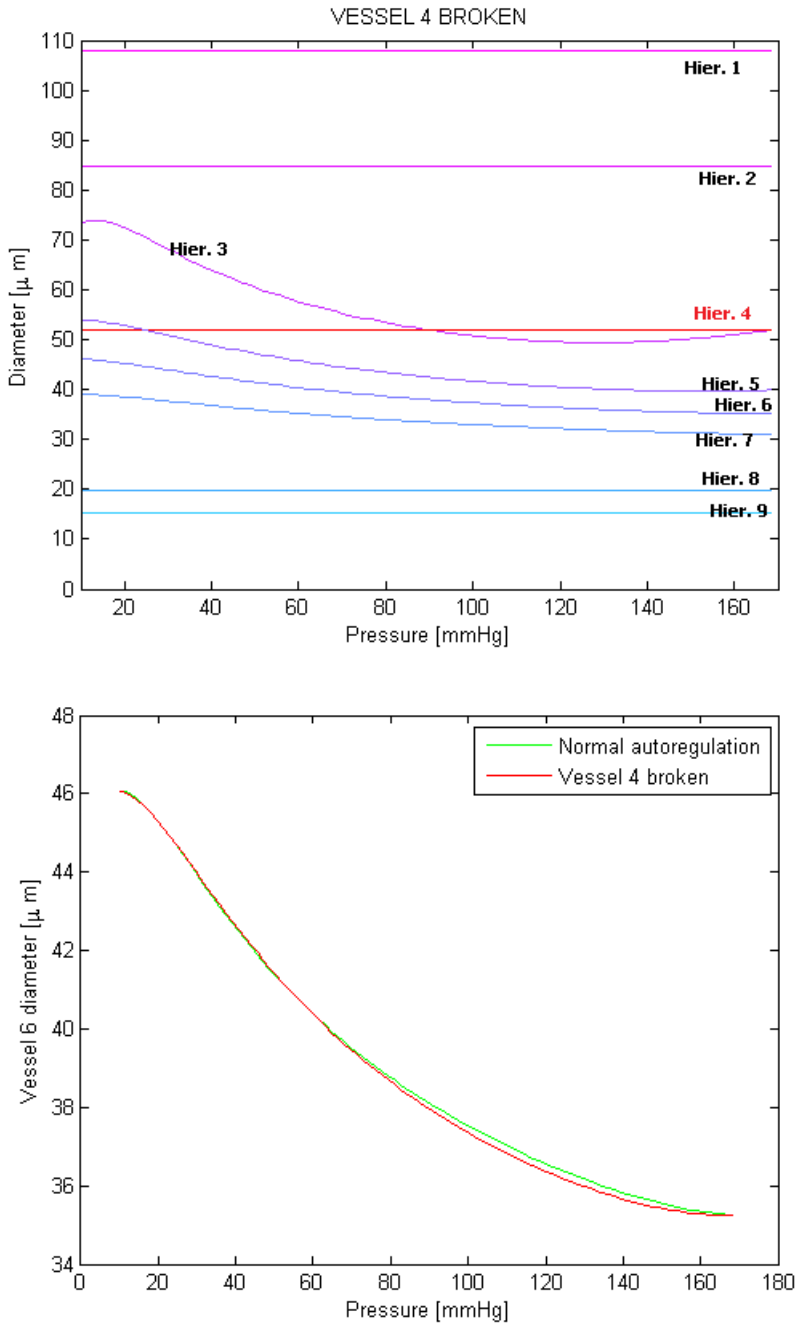

Figure 4.5: Top figure: a pressure vs diameter plot for a system with 8 hierarchy, with autoregulating level from 3 to 7 and vessel 4 broken (red line: the vessel does not react to the pressure changes, thus its diameter remains constant in time). Bottom figure: in-detail effects of the presence of the broken level on vessel 6 diameter.

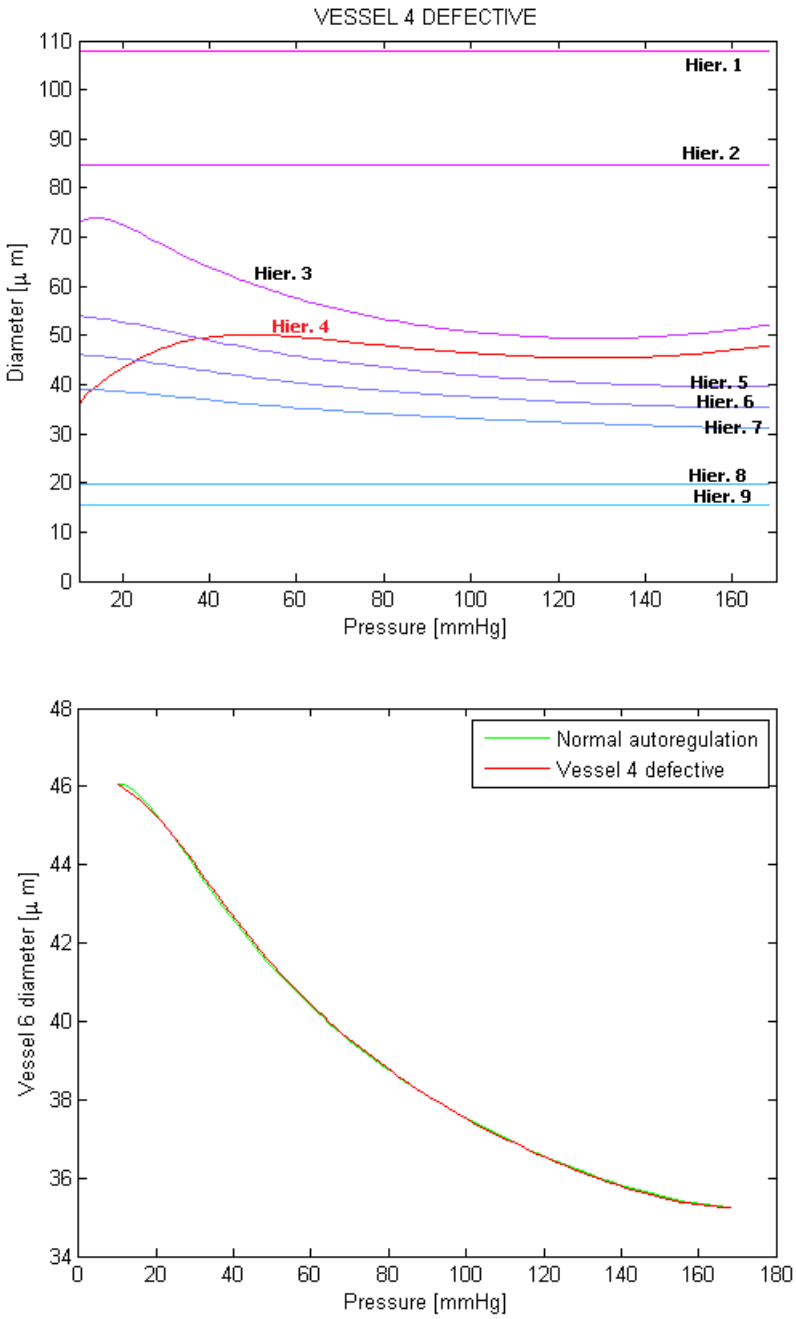

Figure 4.6: Top figure: a pressure vs diameter plot for a system with 8 hierarchy, with autoregulating level from 3 to 7 and vessel 4 defective (red line: the vessel react with delay to the changes of pressure, thus its diameter's changes are smaller). Bottom figure: in-detail effects of the presence of the defective level on vessel 6 diameter.

4.1.5 Effects of varying the type of autoregulation on a single vessel.

As seen in chapter 3, different type of autoregulation can affect the changes in diameters, and we had visualized this differences in Figure 3.11 and 3.10, which represented the trend of the diameters in dependence of time and of the autoregulatory responses activated. In Figure 4.7 and 4.8 the different equilibrium diameter values are plotted in dependence of different inlet pressure levels on vessel of hierarchy 3 and 6. The wall shear tension at control state used in the shear-dependent autoregulation has been considered equal to 55dyn/cm from data found in [1]. As fot the metabolic response, we remember that oxygen is delivered to surrounding tissues by an upstream artery, large arterioles, small arterioles and capillaries. Oxygen exchange by venules and veins is neglected. A Krogh-type cilinder model is used in which each oxygen-delivering vessels runs along the axis of a cylinder representing a tissue region to which it is exclusively responsible for supplying oxygen. The conducted response signal S_{CR}, which influences the parameter S_{tone} in metabolic autoregulation, usually obtained by the integral of the ATP concentration along the vascular pathway, is taken in our test at a value of approximately 0.45, corresponding to moderate exercise oxygen demand from tissue as far as 2cm.

We can see that for both vessels the diameter equilibrium slightly differs from one response type to another, with a deviation of $\simeq 10\mu$m for lower pressure to a deviation of $\simeq 2/5\mu$m for higher pressure. The response that seems to influence more the vaso-contraction is the myogenic one.

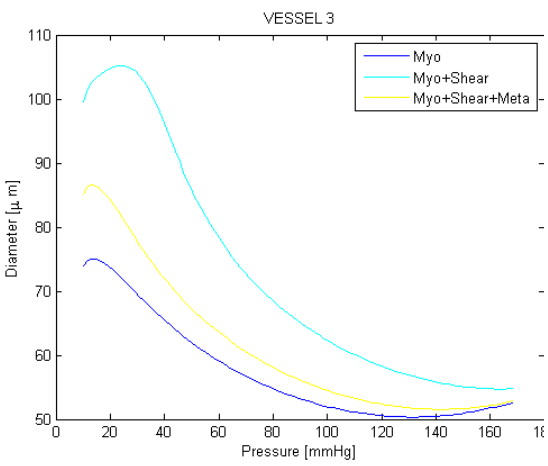

Figure 4.7: Pressure vs. diameter plot for vessel 3.

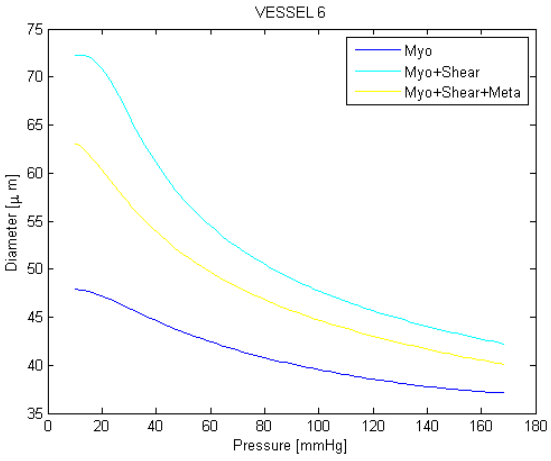

Figure 4.8: Pressure vs. diameters plot for vessel 6.

4.1.6 Cumulative resistance

Using its analogies with the electrical circuits, we have computed the cumulative resistance of the microvascular network at each hierarchical level; the results had been obtained by summing in parallel the resistances in the node of the same hierarchy to then sum it in series with the ones of the previous hierarchies. The cumulative resistance is plotted in Figure **??** as a function of the branching level. The majority of resistance is obtained at the first branch level, while after approximately level 10 the increase in resistance is reduced. That suggests that extending the tree to a larger number of branches becomes non influential after a certain number of levels for the resistance, which reaches an asymptotic value.

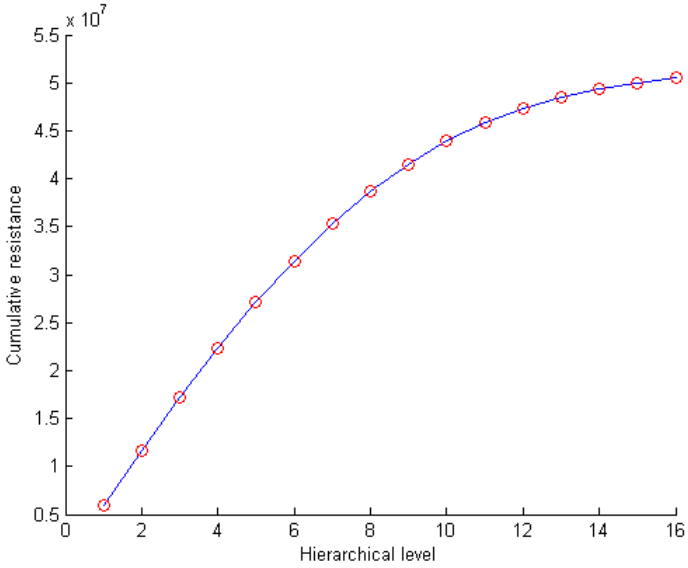

Figure 4.9: Branching level vs. cumulative resistance.

Chapter 5

Homogenized model for microvascular network

In Ch. 2 the retinal microvasculature was represented with a network model based on a dichotomous tree. Of course in the reality the microvascular network is much more complicated than that: that is why homogenized model constitute a better approach. In this chapter we are presenting two ways to apply homogenized models to the retinal microvasculature: the first one supposes that Darcy's law can be used only for the deeper layers of the retina, whereas in the other layers the major vessels can be treated using the Poiseuille law. The second way divides the entire retinal microvasculature in a hierarchical structure, as done in works by Vankan and Huyge ([32],[33]) and as used in subsequent works ([11]).

5.1 Darcy model

As previously said, the vascular network is organized in a hierarchical way. Most of the relevant transfer processes between blood and tissues are due to small vessels, that means arterioles and capillaries. Some examples of these processes are oxygen delivery, carbon dioxide removal and transfer of other chemicals.

In focusing on modeling of perfusion and mass transport in tissues, an appropriate mathematical approach is to use Navier-Stokes or other accurate models for large vessels, while reduced models for the remaining part of the circulation.

So we will consider blood flow at *macroscale* in large and medium sized vessels, that one wants to describe taking in account their geometry. The macroscale models are given by complex arterial trees, the blood flow is

assumed to be fast and mass transport takes place. Their geometrical complexity asks for models apt to resolve the vessel geometry and capture the behavior of the main physiological variables (blood pressure, concentrations, temperature..): 1D models seem to be the best choice.

But when the vessels become too small, we choose in a way to ignore their geometry and other fine properties, which are not known in detail: so when we are in small vessels and capillary beds we take the blood flow at *microscale*. In this models the blood flow is supposed to be slow, and transfer processes between tissue and vessels take place. Only *averaged* quantities are used since the exact conformation of vessels is not taken into account. To represent all the directions in which the blood perfuses 3D models are the best choice.

Of course the macroscale and microscale models are not independent: they are supposed to communicate with each other since the blood perfusing at microscale in the tissues comes from larger vessels at macroscale, so the 1D domain for larger vessels is assumed to be a subset of the 3D tissue domain. This leads to the sometimes complicated problem of the coupling conditions at boundaries where macroscale ends up in microscale.

The microscale/macroscale models can be applied directly to the case of the retinal vessels. Remembering that the retinal vasculature is divided in three layers, the idea is that the superficial and intermediate vasculature should be treated considering the macroscale model and Poiseuille law for large vessels whose geometry cannot be ignored, while the perfusion in the vessel of the deeper layer, whose diameters become too small, can be approximated using the microscale model. This division is well visualized in Figure 5.1.

5.1.1 Darcy's law

We will be considering in our analysis the case of single phase flow in a porous medium, where with *phase* we mean a matter that has a homogeneous chemical composition and physical state (solid, liquid, gas). The governing equations for a single phase flow in a porous medium are given by:

- conservation of mass
- Darcy's law
- equation of state

The conservation of mass is expressed by the following equation:

$$\frac{\partial(\phi\rho)}{\partial t} = -\nabla(\rho u) + q \tag{5.1}$$

where ϕ is the *porosity* of the medium, ρ is the density of the fluid per unit volume, and q represents the external sources and sinks. The vector $u = (u_1, u_2, u_3)$ is the superficial *Darcy velocity*, and we get it from the momentum conservation equation in the form of Darcy's law:

$$u = -\frac{1}{\mu} k \nabla p \tag{5.2}$$

where k is the absolute permeability tensor, μ the fluid viscosity. Substituting Eq.(5.2) in Eq.(5.1) yields:

$$\frac{\partial(\phi\rho)}{\partial t} = \nabla \cdot (\frac{\rho}{\mu} k \nabla p) + q \tag{5.3}$$

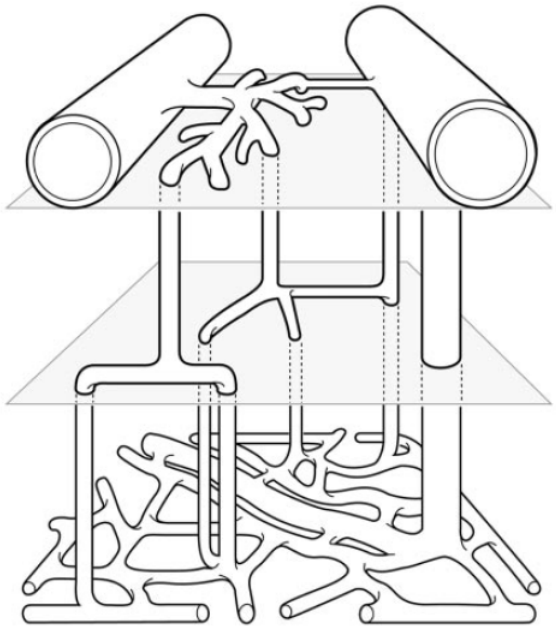

Figure 5.1: Schematic representation of the micro and macro vessels structure in the retina. The arteriole is on the top left, the venule in the top right. In the deep layer the vessels becomes to small, and to describe the blood flow there the extensions of Darcy law for multiporous media could be used. (Figure taken from [38])

We are now going to consider two different ways to interpret the flow in porous media, differing in the way the flow is supposed to pass through the media: the hydraulic radius model and the capillary bundle model. The starting point in our analysis, whatever the capillary distribution, will be the Hagen-Poiseuille law for steady flow through a single straight circular capillary tube:

$$Q_s = -\frac{\pi\delta^4\rho g}{128\mu}\frac{\partial p}{\partial s} \tag{5.4}$$

$$V_s = \frac{Q_s}{\pi\delta^2/4} = -\frac{\rho g}{\mu}\frac{\partial p}{\partial s} \tag{5.5}$$

where p is the pressure, s is the length measured along the tube, δ the tube diameter, Q_s the total discharge, V_s the average velocity in the tube. We can find a connection between this formula and the Darcy's law as expressed before by identifying $\frac{\delta^2}{32}$ with the permeability k. Any development of the models based on Hagen-Poiseuille law will eventually lead to a linear relationship between velocity and the piezometric head gradient. The models will differ just in the relationship they yield among permeability k and the properties of the media.

5.1.2 Hydraulic radius model

The model of the hydraulic radius is a *drag model*: that means the flow in the porous media is assumed to be around solid objects immersed in the fluid. The model has shown to be the best choice for high porosity values (for example powders), and is regarded as a phenomenological approach. Its theory has been developed mainly by Carman and Kozeny in [7]: in their model the porous medium is assumed to be equivalent to a conduit whose cross section has an extremely complicated shape, but with a constant area on the average, and the flow is supposed to be laminar.

The *hydraulic radius* R is defined as:

$$R = \frac{\text{void volume of the medium}}{\text{surface area of the channels in medium}}$$

The channel diameter d_H governing the flow rate through the conduit is in the end assumed to be four time this hydraulic radius, that is $d_H = 4R$. We get the average pore velocity v_p in the flow channels from a Hagen-Poiseuille equation type

$$v_p = \frac{\Delta p}{L_e}\frac{d_H^2}{k_0 16\mu}$$

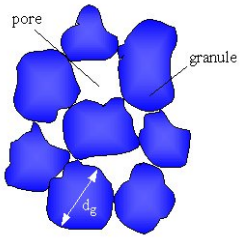

Figure 5.2: Drag model: the fluid flows around the granules, each with a radius d_g.

where L_e is the average path length of flow, k_0 is a shape factor, and Δp is the pressure drop over the distance L_e. Reminding that the filter velocity v in Darcy's law was:

$$v = \frac{k}{\mu}\frac{\Delta p}{\Delta L}$$

These two velocities are related as follows:

$$v_p = \frac{v}{\phi}\frac{L_e}{L} = v_{DF}\frac{L_e}{L} \tag{5.6}$$

The division if v by the porosity ϕ is the "Dupuit-Forchenheimer assumption", which is very often used to define an average interstitial velocity. The multiplication of v by L_e/L is due to Carman: it corrects for the fact that a hypothetical fluid particle used in the microscopic flow equations and flowing with velocity v covers a path length L in the same time as an actual fluid particle flowing with velocity v_p covers an average effective path length L_e. Combining the previous equation we find the expression for the *Carman-Kozeny constant* k_{CK}:

$$k_{CK} = \phi\frac{d_H^2}{16k_0}(\frac{L_e}{L})^2 \tag{5.7}$$

We can relate the hydraulic diameter with the specific surface area S_0 based on the solid volume:

$$d_H = 4\frac{\phi}{S_0(1-\phi)} \tag{5.8}$$

Combining eqs 5.7 and 5.8 the usual form of the Carman-Kozeny equation for permeability is obtained:

$$k_{CK} = \frac{\phi^3}{k_0(L/L_e)^2(1-\phi)^2S_0^2} \tag{5.9}$$

where $(\frac{L}{L_e})^2$ is used to be called *tortuosity factor* τ. The hydraulic tortuosity factor τ is not a property of the porous medium, but it is a parameter of the one-dimensional model of the medium: if the length in the direction of macroscopic flow is L, the porosity ϕ, the pressure drop Δp, and the flow rate Q, the capillary model consists of tubes of length L whereas the effective length of pores in the medium is $L_e > L$. Therefore, in the medium the pore velocity for given Δp is L/L_e times less, just like the number of pores.

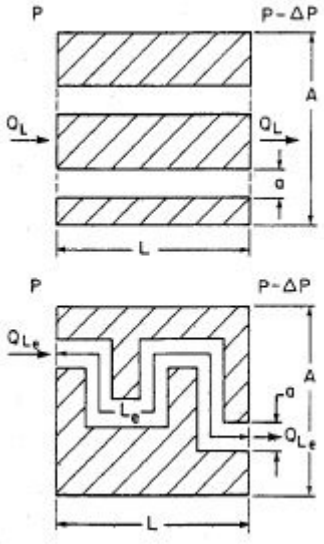

Figure 5.3: Illustration of the physical meaning of the 'tortuosity factor'. $Q_L/Q_Le = (L_e/L)^2 = \tau$. (Figure taken from [14])

5.1.3 Capillary bundle model

The model of the capillary bundle is a *capillary model*. The flow in the porous media is regarded as a flow through tortuous conducts. In our first analysis we will consider the case of a bundle of **identical** N capillaries, assuming a cube shaped sample of length L; the capillaries are all assumed to be of length L and diameter d, and satisfying the condition of porosity:

$$\phi = N\frac{d^2\pi}{4L^2} \tag{5.10}$$

We can express the flow rate Q under the influence of the pressure drop Δp given by the Hagen-Poiseuille law equation:

$$Q = N\frac{d^4\pi}{128\mu}\frac{\Delta p}{L} \tag{5.11}$$

and confront it with the same equation given by Darcy's law:

$$Q = \frac{k_1}{\mu} L^2 \frac{\Delta p}{L} \tag{5.12}$$

Combining equations 5.10, 5.11 and 5.12 gives us the expression of the permeability k_1 in this one-dimensional model:

$$k_1 = \phi \frac{d^2}{32} \tag{5.13}$$

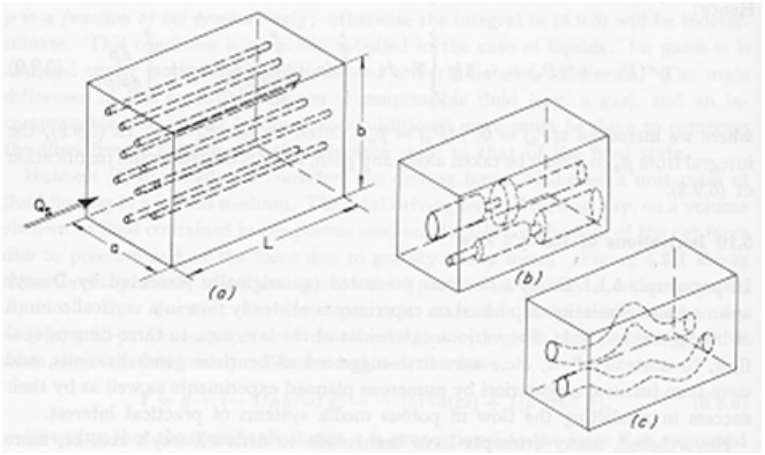

Figure 5.4: Different capillary models: the medium is seen as a block crossed by conducts in which the fluid can flow. (a) identical straight parallel capillaries with constant diameter. (b) straight capillaries with varying diameters. (c) non-straight capillaries. (Figure taken from [3])

Now we want to build a **pseudo three dimensional** capillary model assuming that the capillaries are not all parallel, but arranged in such a way that $N/3$ capillaries would be parallel to the x-axis, $N/3$ parallel to the y-axis and $N/3$ parallel to the z-axis. This model is isotropic and more realistic than the previous one, and its permeability k, for the same given porosity ϕ, is $1/3$ of the permeability k_1 of the one-dimensional model:

$$k = \frac{k_1}{3} = \phi \frac{d^2}{96} \tag{5.14}$$

By orienting pores with equal probability in the three space coordinate directions a *hydrodinamic tortuosity* factor $\tau = 3$ has been introduced into the model. We see that the permeability k diminishes by the factor τ since the flow in a medium where the conducts are oriented in different direction

is supposed to be more difficult.

Scheidegger made some improvements of this model (see [40]), firstly by considering a bundle of N parallel capillaries, but with **different diameters**. Each capillary is assumed to have a uniform cross section and the frequency of each diameter δ is given by a volume based *pore size density* $\alpha(\delta)$. To be more precise, if we define $\alpha(\delta)d\delta$ as the fraction of the pore volume made up of pores whose diameter is $\in (\delta, \delta + d\delta)$, the relation with the volume is:

$$V = \frac{1}{3} N \Delta x_i \alpha(\delta) d\delta$$

Once again we obtain permeability of this capillary model by comparing with Darcy'law as follows:

$$k = \frac{\phi}{96} \int_0^\infty \delta^2 \alpha(\delta) d\delta \tag{5.15}$$

We must say that the value for the diameter calculated in 5.15 is extremely sensitive to errors at the extremity of the pore size distribution function, corresponding to the largest pores size. Moreover if the pore entry size distribution is used the model will be very different from the actual pore structure.

5.2 Hierarchical mixture theory

An alternative approach to using Darcy's law only for capillary bed is the one used in [11], in which not only the vessels in the lower layer of the retina follows Darcy's law, but the entire retinal microvasculature. All the vessel we are considering in the retina are supposed to follow a hierarchical structure: they belong to several branching orders with their specific properties, depending on their radius. So for variables like hydraulic tissue permeability, porosity, and mean flow velocity we consider a distribution of values instead of a single value, depending on the level of the hierarchy the vessel occupies. Let $\theta \in [-1, 1]$ be the *hierarchical parameter* which represents the level a given vessel belongs. Negative values correspond to the veins: from 0 to -1 the vein diameters get progressively larger. The value 0 corresponds to the smallest vessels (capillaries), while the positive values from 0 to 1 correspond to progressively larger arteries.

Each unknown related to blood flow depends both on:

- the spatial variables, for the movements through vessels of comparable porosity

- the hierarchical coordinate θ, for the movements from a hierarchical level to a lower one.

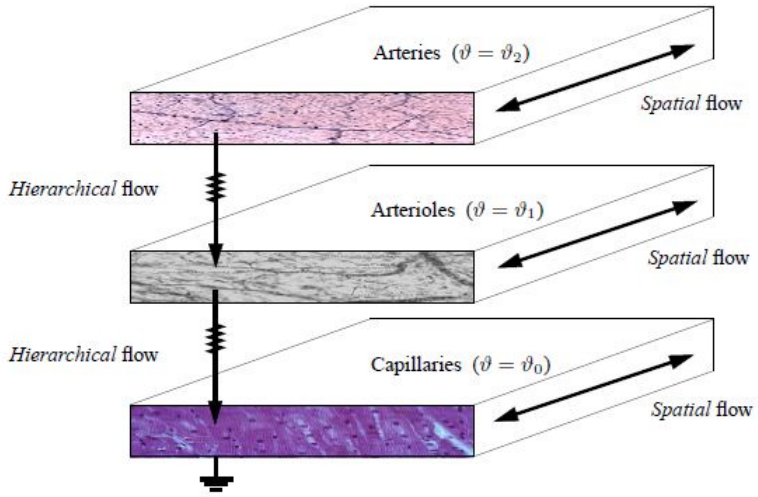

Figure 5.5: A 3D example of the hierarchical model - arteries, arterioles and capillaries are taken into account. (Figure taken from [11])

Mixture theory has proven to be a valuable means to model the mechanical behavior of biological tissue: in this theory the various solid and fluid components of the tissue are modeled as interacting continua. An important fluid components in biological tissue is of course blood, and it is responsible as we had said for then nutrition and drainage processes that are essential for the tissue. Blood flows in the hierarchical system we have presented in Figure 5.2, called the vascular tree.

Because of this hierarchical architecture blood flow cannot be adequately described by biphasic mixture theory: the state of blood depends strongly on the position in the hierarchy. For example, the velocity and pressure in the capillary blood are much lower than the ones of the arterial blood.

In [47], Huyghe and Vankan use mixture theory to derive the fundamental conservation equation in a general context of hierarchical porous media. The tissue is modeled as a mixture of one solid and one fluid, where the fluid represents the blood. The fluid is subdivided into a number of compartments, each of which represents the blood on a different hierarchical position in the vascular tree. Blood flow through vasculature is described as communication between the fluid compartments, which corresponds with the physiological definition of *perfusion*: the volume of blood passing a given level in the vascular hierarchy per unit of volume per volume of tissue. Vessel walls are

modeled as an elastic solid-fluid interface, and give a local contribution to the pressure difference between solid and fluid.

5.2.1 Conservation of mass

The mass conservation equation derived by Bowen in [6] for mixture theory with n incompressible immiscible fluids saturating one incompressible solid is, for each phase:

$$\frac{\partial N^i}{\partial t} + \nabla \cdot (N^i V^i) = \Theta^i \qquad i = 1, \ldots, n$$

where N^i is the volume fraction, V^i the velocity, Θ^i the volume fluid interaction of phase i. We will assume that the position in the hierarchy is quantified by the dimensionless parameter θ, and that for each phase the communication between the fluid compartments is described by the fluid volume interaction Θ^b from the previous equation. A fluid compartment defined by the hierarchical range $[\theta, \theta + d\theta]$ has a volume fraction $n^b d\theta$ in which n^b represents the fluid (blood) volume fraction per unit hierarchical parameter, that means the porosity of the hierarchical compartment. So the mass balance for the fluid compartment θ is:

$$\frac{\partial n^b}{\partial t} d\theta + \nabla \cdot (n^b v^b) d\theta = n^b(\theta)\omega(\theta) - n^b(\theta + d\theta)\omega(\theta + d\theta)$$

where the right side represents the volume interaction with the neighboring compartments, ω is the measure of the rate at which blood flows from one compartment to the next, and is defined as the material time derivative of θ, and $n^b\omega$ corresponds to the traditional physiological definition of regional blood perfusion. Dividing the equation for θ yields for infinitesimal θ the local fluid mass balance:

$$\frac{\partial n^b}{\partial t} + \nabla \cdot (n^b v^b) = \tilde{\Theta}^b = -\frac{\partial (n^b)\omega}{\partial \theta} \tag{5.16}$$

where $\tilde{\Theta}^b$ is the volume fraction for unit hierarchical parameter. Remembering that the total mass balance of the mixture implies $\sum_i \Theta^i = 0$, assuming no mass interaction between solid and fluid this can be rewritten as:

$$\Theta^s = \int_{-1}^{1} \tilde{\Theta}^b d\theta = 0$$

The saturation of the mixture is expressed as

$$N^S + \int_{-1}^{1} n^b d\theta = N^S + N^b = 1$$

which, combined with the previous equations gives the solid and fluid total mass conservation in their new expressions:

$$-\frac{\partial N^b}{\partial t} + \nabla \cdot ((1 - N^b)V^S) = 0 \tag{5.17}$$

$$\frac{\partial n^b}{\partial t} + \nabla_4 \cdot (n^b \mathbf{v_4}) = 0 \tag{5.18}$$

where ∇_4 and $\mathbf{v_4}$ are four-dimensional operator and vector:

$$\nabla_4 = \begin{bmatrix} \frac{\partial}{\partial \theta} \\ \nabla \end{bmatrix} \qquad \mathbf{v}_4 = \begin{bmatrix} \omega \\ \mathbf{v} \end{bmatrix}$$

5.2.2 Darcy's model in tissue perfusion

As mentioned before, we will consider the tissue domain as an $\Omega \subset \mathbb{R}^3$, and Ω_b as the subdomain occupied by blood vessels, that are the pores of the medium. The average variables on the domain are defined by means of a *reference elementary volume* (REV), a four dimensional quantity (three dimension in space, one in hierarchy). His size h_{REV} is considered negligible with respect to the characteristic lengths of the macroscale, but still large enough to allow a meaningful averaging. So, for a generic point $(\mathbf{x}, \theta) \in \Omega \times [0, 1]$ we define the REV as:

$$\mathcal{U}_0 = \{(\mathbf{x}', \theta') \in \Omega_b \times [-1, 1] : ||(\mathbf{x}', \theta') - (\mathbf{x}, \theta)|| < h_{REV}\}$$

The microscopic physiological variables defined on Ω_b are:

- p_b pore pressure
- $\mathbf{v}_b$ pore spatial velocity, defined by $\mathbf{v}_b = \frac{Dx}{Dt}$ (material derivative).
- ω_b pore hierarchical velocity, defined by $\omega_b = \frac{D\theta}{Dt}$. This quantity represents the rate at which blood moves in the hierarchy: note that in normal condition the value will be negative since blood moves down to lower level of the hierarchy.

We can get now macroscopic variables on the whole Ω by averaging the microscopic ones:

- $p = p(t, \mathbf{x}, \theta) = \frac{1}{|\mathcal{U}_0|} \int_{\mathcal{U}_0(\mathbf{x},\theta)} p_b(t, \mathbf{x}', \theta') d\mathbf{x}' d\theta'$ mean blood pressure.
- $\mathbf{v} = \mathbf{v}(t, \mathbf{x}, \theta) = \frac{1}{|\mathcal{U}_0|} \int_{\mathcal{U}_0(\mathbf{x},\theta)} \mathbf{v}_b(t, \mathbf{x}', \theta') d\mathbf{x}' d\theta'$ mean spatial blood velocity.

- $\omega = \omega(t, \mathbf{x}, \theta) = \frac{1}{|\mathcal{U}_0|} \int_{\mathcal{U}_0(\mathbf{x},\theta)} \omega_b(t, \mathbf{x}', \theta') d\mathbf{x}' d\theta'$ mean hierarchical blood velocity.

Using the fundamental conservation laws and the mixture theory elements results we get the system which describes blood perfusion, a four-dimensional Darcy equation:

$$\begin{cases} \frac{\partial n^b}{\partial t} + \nabla \cdot (n^b \mathbf{v}) + \frac{\partial}{\partial \theta}(n^b \omega) \\ n^b \mathbf{v} = -K_t \nabla p \\ n^b \omega = -\alpha \frac{\partial p}{\partial \theta} \end{cases} \tag{5.19}$$

where $t > 0$, $(\mathbf{x}, \theta) \in \Omega \times [0, 1]$. The first equation expresses the conservation of fluid mass, the second one the conservation of fluid momentum. The border conditions are:

$$\begin{cases} n^b \omega(t, \mathbf{x}, -1) = G_0(p(t, \mathbf{x}, 0) - p_v(t, \mathbf{x})) \\ n^b \omega(t, \mathbf{x}, 1) = G_1(p(t, \mathbf{x}, 0) - p_a(t, \mathbf{x})) \\ n^b \omega(t, \mathbf{x}, \theta) \cdot n = 0 \end{cases} \tag{5.20}$$

Analyzing in detail the quantities we have introduced:

- $n^b = n^b(\mathbf{x}, \theta)$ is the porosity, defined ad the ratio between the blood volume $|\mathcal{U}_0|$ and the total volume (blood + tissue) in the REV, in other words the fluid fraction.

- $$\tilde{K}(\mathbf{x}, \theta) = \begin{bmatrix} K(\mathbf{x}, \theta) & 0 \\ 0 & \alpha(\mathbf{x}, \theta) \end{bmatrix}$$
  is the four dimensional hierarchical permeability tensor: it can be computed experimentally, but also theoretically from the microscale geometry.

- q is the generic tissue fluid loss term.

- G_0 is the hydraulic conductivity between the lowest hierarchy and the draining veins, while G_1 between the highest hierarchy and the feeding arteries.

- p_a and p_v are the functions describing the arterial and venous pressure in the tissue region, and are different from 0 only where the feeding arteries and draining veins are located.

The difference between this model and the one used by D'Angelo in [11] is that here the compliance effect of the vessel walls is not accounted: we are considering just autoregulation.

5.2.3 Coupling with autoregulation

We now have to connect at each time the hierarchical fluid volume fraction n^b with the autoregulation mechanism, as we have done before with the network model. The porosity n^b and the permeability K can be connected with the diameter using the expression found in the chapter about the capillary bundle model.

The porosity n^b can be computed as

$$n^b(\mathbf{x}, \theta, t) = \frac{N(\theta)\pi D^2(\mathbf{x}, \theta, t)L(\theta)}{4V_{tot}} \tag{5.21}$$

where N is the number of vessels in the volume, and v_{tot} the total volume. We will assume that N and L are constant in time and depend only on the hierarchy level θ.

The permeability is the measure of the ability of a porous medium to allow fluids to pass through it: spatial permeability K refers to flows within the same hierarchical level, in contrast to hierarchical permeability α, which refers to the flow between different hierarchical levels. We suppose that the permeability tensor K is space-independent and isotropic, so that:

$$K = K(\theta)I$$

where $K(\theta)$ is a scalar function, the values of which can be obtained from standard data, and I the identity tensor. The Darcy velocity as expressed in equation 5.19 in dependence of the pressure drop in the vessel δp and the vessel length δl is:

$$n^b v = k\frac{\delta p}{\delta l}$$

The blood flow velocity can be expressed also thanks to the Poiseuille law as:

$$v = \frac{D^2}{32\mu}\frac{\delta p}{\delta l}$$

where μ is the dynamic blood viscosity and r is the vessel radius. Combining the two previous equations we get the permeability:

$$K(\mathbf{x}, \theta, t) \simeq n^b(\mathbf{x}, \theta, t)\frac{D(\mathbf{x}, \theta, t)^2}{32\mu(\theta)} \tag{5.22}$$

Having expressed the porosity n^b as a function of D, we write:

$$\frac{\partial n^b}{\partial t} = \frac{\partial n^b}{\partial D} \cdot \frac{\partial D}{\partial t}$$

to be inserted in the mass conservation relation in 5.19. Calculating it explicitly:

$$\frac{\partial n^b}{\partial t} = \frac{\partial n^b}{\partial D} \cdot \frac{\partial D}{\partial t} =$$
$$= \frac{N\pi DL}{V_{tot}} \cdot \frac{\partial D}{\partial t} = \frac{N\pi LD}{V_{tot}} \left[\frac{D_c}{\tau_d T_c} (T - T_{total}) \right]$$

Substituting this value in the mass conservation law, at timestep k we have:

$$\nabla \cdot (-K^{(k)} \nabla p) + \frac{\partial}{\partial \theta} \left(\alpha \frac{\partial p}{\partial \theta} \right) = f^{(k)} \tag{5.23}$$

where

$$K^{(k)} := \frac{n_b^{(k)} (D^{(k)})^2}{32\mu}$$
$$f^{(k)} := -\frac{N\pi L}{V_{tot}} D^{(k)} \left[\frac{D_c}{\tau_d T_c} (T^{(k)} - T_{total}^{(k)}) \right]$$
$$T^{(k)} = \frac{(p^{(k)} - IOP) D^{(k)}}{2h}$$
$$T_{total}^{(k)} = T_{pass} + A^{(k)} T_{act}^{max}$$

Resolving equation 5.23 we get the parameters $n_b^{(k+1)}$ and $p^{(k+1)}$. The second in particular can be used for the computation of the other variables $A^{(k+1)}$ and $D^{(k+1)}$ via the autoregulation model:

$$\begin{cases} \dfrac{dD}{dt} = \dfrac{D_c}{\tau_d} \left[\alpha^{(k+1)} D - T_{act}^{max} A \right] \dfrac{1}{T_c} - \dfrac{D_c}{\tau_d} \dfrac{T_{pass}}{T_c} \\ \dfrac{dA}{dt} = \dfrac{1}{\tau_a} \dfrac{1}{1 + e^{-\beta^{(k+1)} D}} - \dfrac{A}{\tau_a} \end{cases} \tag{5.24}$$

which is a non-linear system, where:

$$\alpha^{(k+1)} := \frac{p^{(k+1)} - IOP}{2h}$$
$$\beta^{(k+1)} := C_{myo} \alpha^{(k+1)}$$

Upon assuming small changing in diameter size, we can try to get a linearized model, using Taylor series around the diameter in control state D_c for the non-linear term $f(D) = 1/1 + e^{-\beta D}$:

$$f(D) \simeq \frac{1}{1 + e^{-\beta D_c}} + \frac{\beta e^{-\beta D_c}}{(1 + e^{-\beta D_c})^2} (D - D_c)$$

The linearized autoregulation model can be written as:

$$\begin{cases} \dfrac{dD}{dt} = \left(\alpha^{(k+1)}\dfrac{D_c}{\tau_d T_c}\right) D - \left(\dfrac{D_c T_{act}^{max}}{\tau_d T_c}\right) A - \dfrac{D_c T_{pass}}{\tau_d T_c} \\ \dfrac{dA}{dt} = \left(\dfrac{\beta e^{-\beta D_c}}{(1+e^{-\beta D_c})^2}\right) D - \left(\dfrac{1}{\tau_d}\right) A - \dfrac{1}{1+e^{-\beta D_c}} + \dfrac{\beta e^{-\beta D_c}}{(1+e^{-\beta D_c})^2} D_c \end{cases} \tag{5.25}$$

The system 5.25, properly choosing the parameters a, b, c, d, e, f can be resolved as a linear system with the MATLAB command `dsolve`, in order to get the results D and A at timestep (k+1).

$$\begin{cases} \dfrac{dD}{dt} = aD + bA + e \\ \dfrac{dA}{dt} = cD + dA + f \end{cases}$$

As for the coefficient α, the hydrodynamic conductance per unit volume between contiguous hierarchical levels, it can be extrapolated assuming to know the mean values $\overline{p}_i$ and $\overline{\omega}_i$ for pressures and hierarchical velocities as follows:

$$\phi\overline{\omega}_i = -\alpha_i \left(\frac{\partial p}{\partial \theta}\right)_{\theta=\theta_i} \simeq -\alpha_i \frac{\Delta \overline{p}_i}{\Delta \theta_i}$$

$$\Longrightarrow \alpha_i \simeq -\phi\overline{\omega}_i \frac{\Delta\theta_i}{\Delta\overline{p}_i}$$

So in conclusion, a possible new development of the problem could be an investigation of the difference and similarities of the results obtained with a new MATLAB code implemented using the Darcy model for perfusion instead of the network model as seen in Ch. 4 coupled with autoregulation.

Conclusions

The aim of this work was to investigate mathematical models for the phenomenon of autoregulation in the retinal microvascular network, and to couple it with network models representing the microvasculature. After a brief overview of the retina and its microvasculature, the autoregulation model [1] by Arciero et al. and the network model [44] by Takahashi et al. were presented, and combined together in a MATLAB code which used the network similarities with electrical circuits to compute the hemodynamic parameters. The results obtained with the several tests performed with this code permitted us to analyze the trend of such retinal parameters (pressure, vessel diameters and resistance).

In the last part of the work, to give an alternative approach, homogenized Darcy models for microvasculature were introduced; an eventual new coupling with autoregulation could be a future new development of this work.

Acknowledgements

I said I wouldn't write this part. But then everyone kept telling me to write this, because it is the only thing people actually read - and I suppose that's the truth. So here they are, acknowledgements.

Thanks to Paola Causin and Riccardo Sacco for the way they have followed me all along this work, being always present and encouraging.

Thanks to my family, my mother Tiziana and my father Angelo - I can't imagine a better family than mine, and that has meant a lot for me during these years.

Thanks to my 'best friends', Alessandra and Luca, so different yet so similar in understanding and always sustaining me when I was being happy, sad, depressed, annoying, whatever else.

Thanks to all the other people I have had to my side - Andrea for all the time we spent together, Federica for her text-messages and dinner at her place, Federico for all the movies and 'crital mass', Ilaria for the VIP-holidays, Patrizia for the interesting conversations in the library. Thanks to everyone else who is reading and is not in the list. Thanks a little even to myself.

Bibliography

[1] Arciero, J.C., Carlson, B.E., Secomb, T.W., *Theoretical model of metabolic blood flow regulation: roles of ATP release by blood cells and conducted responses*, Am. J. Phy. Heart Circ. Phy., **295** H1562 (2008)

[2] Arciero, J.C., Carlson, B.E., Secomb, T.W., *Theoretical model of metabolic blood flow regulation: roles of myogenic, shear dependent, and metabolic responses*, Am. J. Phy. Heart Circ. Phy., **295** H1572 (2008)

[3] Bear, J., *Dynamics of Fluids in Porous Media*, (1972)

[4] Bill, A., Sperger, G.O., *Control of retinal and choroidal bloodflow.* Eye **4** (1990)

[5] Bill, A., Sperger, G.O., *Aspects of oxygen and glucose consuption in the retina: effetcs of high pressure and light.* Graefes Arch. Clin. Exp. Opht. **228**, (1990).

[6] Bowen, R.M., Int. J. Eng. Sci., **18**, 1129 (1980)

[7] Carman, P.C., *Fluid flow through a granular bed*, Trans. Inst. Chem. Eng. London, **15**,150-156 (1937)

[8] Carlson, B.E., Secomb, T.W., *A theoretical model for the myogenic response based on the mechanics of vascular smooth muscle.* Microcirculation, **12**, 327338 (2005)

[9] Charlson, M., *A New View of Normal Tension Glaucoma: Autoregulation and Systemic Blood Pressure* (2011)

[10] Cornelissen, A.J., Dankelman, J., VanBavel, E., Spaan, J.A., *Balance between myogenic, flow-dependent, and metabolic flow control in coronary arterial tree: a model study.* Am J Physiol Heart Circ Physiol, (2002)

[11] D'Angelo, C., *Multiscale modeling of methabolism and transport phenomena in living tissues,* PhD Thesis (2007)

[12] David, T., Alzaidi, S., Farr, H., *Coupled autoregulation models in the cerebro-vasculature.*, J Eng Math, **64** 403-415 (2009)

[13] Duling, B.R., Damon, D.H., *Microvascular responses to alterations in oxygen tension.* Circ Res **31**, 481-489 (1972)

[14] Dullien, F.A.L., *Porous media: fluid transport and pore structure*, (1992)

[15] Ellsworth, M.L., *The red blood cells as an oxygen sensor: what is the evidence?*, Acta Physiol. Scand. **168**, 551-559 (2000)

[16] Ellsworth, M.L., *Red blood cells derived ATP as a regular skeletal muscle perfusion*, Med. Sci. Sports. Exerc. **36** 35-41 (2004)

[17] Evans, D.W., Harris, A., *Glaucoma patients demonstrate faulty autoregulation of ocular blood flow during posture change.*, Br. J. Ophtalmol., **83**, (1999).

[18] Friebel, M., Klotz, K.F., Ley, K., Gaehtgens, P., Pries, A.R., *Flow-dependent regulation of arteriolar diameter in rat skeletal muscle in situ: role of endothelium-derived relaxing factor and prostanoids.* J. Physiol. **483** 715-726 (1995)

[19] Fry, B., *Time dependent myogenic behavior of arterioles*, (2009)

[20] Fung, Y.C., Biomechanics: Circulation. Second edition. Springer-Verlag; New York. (1997)

[21] Ganesan, P., He, S., Xu, H., *Development of an Image-Based network model of retinal vasculature*, Ann of Bio Eng, **38** 1566-1585 (2010)

[22] Ganesan, P., He, S., Xu, H., *Development of an Image-Based network model for capillary vasculature of retina*, (2010)

[23] Gonzalez-Fernandez, J.M., Ermentrout, B., *On the origin and dynamics of the vasomotion of small arteries.*, Math Biosci,**119**, 127167 (1994)

[24] Groebe, K., *Precapillary servo control of blood pressure and postcapillary adjustment of flow to tissue metabolic status. A new paradigm for local perfusion regulation.* Circulation, **94** (1996)

[25] Jackson, W.F., *Arteriolar oxygen reactivity: where is the sensor?* Am J Physiol, **253**, H1120 (1987) H1126.

[26] Johnson, P.C., *The myogenic response.* American Physiological Society; Bethesda, MD: 409-442 (1980).

[27] Johnson, P.C., Intaglietta, M., *Contributions of pressure and flow sensitivity to autoregulation in mesenteric arterioles.* Am J Physiol, **231**, 16861698 (1976)

[28] Harris, A., Ciulla, T.A., Chung, H.S., Martin, B., *Regulation of Retinal and Optic Nerve Blood Flow.* Arch. Ophthalmol.,**116**, 1491-1495, (1998)

[29] Haynes, R.H., *Physical basis of the dependence of blood viscosity on the tube radius* Am. J. Physiol. (1960)

[30] Huyghe, J.M., Oomens, C.W., Van Campen, D.H., Heethaar, R.M., Biorheology, **26**, 55 (1989)

[31] Huyghe, J.M., Oomens, C.W., Van Campen, D.H., Biorheology, **26**, 73 (1989)

[32] Huyghe, J.M.R.J., Van Campen, D., *Finite deformation theory of hierarchically arranged porous solids - I: balance of mass and momentum.* Int. J. Eng. Sci., **33**, 1861-1871 (1995)

[33] Huyghe, J.M.R.J., Van Campen, D., *Finite deformation theory of hierarchically arranged porous solids - II: constitutive behaviour..* Int. J. Eng. Sci., **33**, 1873-1886 (1995)

[34] Kuo, L., Chilian, W.M., Davis, M.J., *Coronary arteriolar myogenic response is independent of endothelium.* Circ Res, **66**, 860866. (1990)

[35] Kuo, L., Davis, M.J., Chilian, W.M., *Endothelium-dependent, flow-induced dilation of isolated coronary arterioles.* Am J Physiol, **259**, (1990)

[36] Liao, J.C., Kuo, L., *Interaction between adenosine and flow-induced dilation in coronary microvascular network.* Am J Physiol, **272** (1997)

[37] Mandecka, A., Dawczynski, J., Vilser, W., Blum, M., *Abnormal retinal autoregulation is detected by provoked stimulation with flicker light in well-controlled patients with type 1 diabetes without retinopathy.* Diabetes Research and Clinical Practice, **86**, 51-55 (2009)

[38] Paques, M., Tadayoni, R., Sercombe, R., *Structural and hemodynamic analysys of the mouse retinal microcirculation*, Investigative Optahlmology Vis. Sc., **44** (2003)

[39] Pohl, U., de Wit, C., Gloe, T., *Large arterioles in the control of blood flow: role of endothelium-dependent dilation.* Acta-Physiol. Scand. **168** 505-510 (2000)

[40] Scheidegger, A.E., *The Physics of Flow through Porous Media*, Univ. of Toronto Press, Toronto, Canada. (1974)

[41] Secomb, T.W., *Theoretical models for regulation of blood flow* Microcirculation, **15** (2008)

[42] Sherman, T.F., *On concerning large vessles to small: the meaning on Murray's law.*J. Gen. Physiol., (1981)

[43] Suwa, N., Takahashi, T.,*Morphological and morphometrical analysis of circulation in hypertension and ischemic kidney*, Munich: Urban&Schwarzenberg (1971)

[44] Takahashi, T., Nagaoka, T., Panagida, H., Saitoh, T., Kamiya, A., Hein, T., Kuo, L., Yoshida, A.,*A mathematical model for the distribution of hemodynamic paramters in the human retinal microvascular network*, J. Biorheol **23**, 77-86 (2009)

[45] Ursino, M., Lodi, C.A., *A simple mathematical model of the interaction between intracranial pressure and cerebral hemodynamics.* J. Appl. Phy. **82**, 1256 (1997)

[46] Ursino, M., Cavalcanti, S., Bertuglia, S., Colantuoni, A., *Vasomotion and blood flow regulation in hamster skeletal muscle microcirculation: A theoretical and experimental study.* Microvasc Res, (1998)

[47] Vankan, W.J., Huyghe, J.M.R.J, Janssen, J.D, Huson, A., *Poroelasticity of saturated solids with an application to blood perfusion*, Int. J. Eng. Sci., **34**, 1019-1031 (1996)

[48] Vankan, W.J., Huyghe, J.M.R.J, Janssen, J.D, Huson, A., Hacking, W., Schreiner, W., *Finite element analysis of blood perfusion through a biological tissue.* Int. J. Eng. Sci., **35**, 375-385 (1997)

[49] White, F.M., *Viscous fluid flow*

[50] Yang, J., Clark, J.W., Jr. Bryan, R.M., Robertson, C., *The myogenic response in isolated rat cerebrovascular arteries: smooth muscle cell model.* Med Eng Phys **25**,691709 (2003)

[51] Yang, J., Clark, J.W., Bryan, R.M., Robertson, C.S., *Mathematical modeling of the nitric oxide/cGMP pathway in the vascular smooth muscle cell.* Am J Physiol Heart Circ Physiol **289** (2005)